OPEN ACCESS

Original research

Targeting m^{6}A reader YTHDF1 augments antitumour immunity and boosts anti-PD-1 efficacy in colorectal cancer

Yi Bao,[1] Jianning Zhai,[1] Huarong Chen ,[2] Chi Chun Wong,[1] Cong Liang,[3] Yanqiang Ding,[1] Dan Huang,[1] Hongyan Gou,[1] Danyu Chen,[1] Yasi Pan,[1] Wei Kang ,[4] Ka Fai To,[4] Jun Yu [1]

► Additional supplemental material is published online only. To view, please visit the journal online (http://dx.doi.org/10.1136/gutjnl-2022-328845).

[1]Department of Medicine and Therapeutics, The Chinese University of Hong Kong, Hong Kong, Hong Kong
[2]Anaesthesia and Intensive Care, Chinese University of Hong Kong, Hong Kong, Hong Kong, Hong Kong
[3]Institute of Precision Medicine, the First Affiliated Hospital, Sun Yat-sen University, Guang Zhou, China
[4]Department of Anatomical and Cellular Pathology, The Chinese University of Hong Kong, Hong Kong, Hong Kong

Correspondence to
Dr Jun Yu, Medicine and Therapeutics, The Chinese University of Hong Kong, Hong Kong, Hong Kong; junyu@cuhk.edu.hk

YB and JZ contributed equally.

Received 5 October 2022
Accepted 17 January 2023
Published Online First 30 January 2023

Check for updates

To cite: Bao Y, Zhai J, Chen H, *et al*. *Gut* 2023;**72**:1497–1509.

ABSTRACT

Objective The role of N^6-methyladenosine (m^{6}A) in tumour immune microenvironment (TIME) remains understudied. Here, we elucidate function and mechanism of YTH N^6-methyladenosine RNA binding protein 1 (YTHDF1) in colorectal cancer (CRC) TIME.

Design Clinical significance of YTHDF1 was assessed in tissue microarrays (N=408) and TCGA (N=526) cohorts. *YTHDF1* function was determined in syngeneic tumours, intestine-specific *Ythdf1* knockin mice, and humanised mice. Single-cell RNA-seq (scRNA-seq) was employed to profile TIME. Methylated RNA immunoprecipitation sequencing (MeRIP-seq), RNA sequencing (RNA-seq) and ribosome sequencing (Ribo-seq) were used to identify YTHDF1 direct targets. Vesicle-like nanoparticles (VNPs)-encapsulated *YTHDF1*-siRNA was used for *YTHDF1* silencing in vivo.

Results *YTHDF1* expression negatively correlated with interferon-γ gene signature in TCGA-CRC. Concordantly, YTHDF1 protein negatively correlated with CD8$^+$ T-cell infiltration in independent tissue microarrays cohorts, implying its role in TIME. Genetic depletion of *Ythdf1* augmented antitumour immunity in CT26 (MSS-CRC) and MC38 (MSI-H-CRC) syngeneic tumours, while *Ythdf1* knockin promoted an immunosuppressive TIME facilitating CRC in azoxymethane-dextran sulphate-sodium or *Apc*$^{Min/+}$ models. scRNA-seq identified reduction of myeloid-derived suppressor cells (MDSCs), concomitant with increased cytotoxic T cells in *Ythdf1* knockout tumours. Integrated MeRIP-seq, RNA-seq and Ribo-seq revealed p65/Rela as a YTHDF1 target. YTHDF1 promoted p65 translation to upregulate CXCL1, which increased MDSC migration via CXCL1-CXCR2 axis. Increased MSDCs in turn antagonised functional CD8$^+$ T cells in TIME. Importantly, targeting YTHDF1 by CRISPR (Clustered Regularly Interspaced Short Palindromic Repeats) or VNPs-si*YTHDF1* boosted anti-PD1 efficacy in MSI-H CRC, and overcame anti-PD1 resistance in MSS CRC.

Conclusion YTHDF1 impairs antitumour immunity via an m^{6}A-p65-CXCL1/CXCR2 axis to promote CRC and serves as a therapeutic target in immune checkpoint blockade therapy.

WHAT IS ALREADY KNOWN ON THIS TOPIC

⇒ N^6-methyladenosine (m^{6}A) modification plays crucial roles in cancer by regulating RNA splicing, translation and degradation.
⇒ YTH N^6-methyladenosine RNA binding protein 1 (YTHDF1) is a m^{6}A reader that determines the fate of m^{6}A modified mRNA. However, its potential role in colorectal cancer (CRC) immune microenvironment (TIME) is understudied.

WHAT THIS STUDY ADDS

⇒ High YTHDF1 expression is inversely correlated with interferon-γ gene signatures and CD8$^+$ T cell infiltration in multiple cohorts of patient with CRC.
⇒ Single-cell sequencing revealed that YTHDF1 contributes to an immunosuppressive TIME with increased infiltration of MDSCs and reduced effector T cells.
⇒ YTHDF1 promotes tumour growth via an immunosuppressive TIME in syngeneic mice, intestine-specific *Ythdf1* knockin mice, and CD34$^+$ humanised mice of CRC.
⇒ Integrative methylated RNA immunoprecipitation sequencing, RNA-seq and Ribo-seq revealed p65/RELA as a YTHDF1 target, leading to increased expression of the cytokine CXCL1, a chemoattractant for MDSCs via CXCL1-CXCR2 axis.
⇒ YTHDF1-recuited MDSCs antagonise effector CD8$^+$ and CD4$^+$ T cells in TIME of CRC, thereby promoting tumourigenesis.
⇒ Targeting of YTHDF1 by gene knockout or nanoparticle-encapsulated *YTHDF1*-siRNA synergised with anti-PD1 to suppress the growth of microsatellite instability-high (MSI-H) CRC, and overcomes anti-PD1 resistance in microsatellite stable (MSS) CRC.

HOW THIS STUDY MIGHT AFFECT RESEARCH, PRACTICE OR POLICY

⇒ Therapeutic targeting of YTHDF1 is a potential strategy to sensitise both MSI-H and MSS CRC to immune checkpoint blockade therapy.
⇒ YTHDF1 serves as a prognostic factor in patients with CRC.

INTRODUCTION

Colorectal cancer (CRC) is one of the most common cancers worldwide. It is still a deadly cancer with a 5-year survival rate lower than 20% among metastatic patients.[1] Immune checkpoint blockade (ICB) has shown beneficial effects to patients with CRC. However, only a minor fraction of patients with microsatellite instability-high (MSI-H) or deficient mismatch repair are responsive to ICB.[1 2] Therefore, understanding the molecular mechanisms of immune evasion in CRC and identifying therapeutic strategies that could improve the response to immunotherapies for patients with proficient mismatch repair, microsatellite instability-low, or microsatellite stable (MSS) CRC are crucial.

N^6-methyladenosine (m^6A) is one of the most abundant RNA modifications, with an estimated 3–5 m^6A sites on each mRNA molecule.[3] m^6A modification is regulated by writers, erasers and readers. m^6A writers catalyse m^6A formation, consisting of a protein complex of METTL3, METTL14 and WTAP. m^6A markers are also actively removed by erasers including FTO and ALKBH5. m^6A readers, such as YTH N^6-methyladenosine RNA binding protein 1/2/3 (YTHDF1/2/3), YTHDC1/2 and IGF2BP1/2/3 bind to m^6A-modified mRNAs to determine the fate of m^6A-modified mRNA.[3] m^6A regulators such as YTHDF1, METTL3 and ALKBH5 have been intensively studied in cancer. Upregulation of YTHDF1 has been reported to be associated with poor prognosis in various cancer types[4–6] and YTHDF1 could promote tumourigenesis and cancer metastasis.[4–6] However, the role of YTHDF1 in tumour immune microenvironment (TIME) is largely unclear.

Here, we identified that *YTHDF1* expression negatively correlated with the interferon gamma (IFN-γ) signature in The Cancer Genome Atlas (TCGA) CRC dataset. Furthermore, we demonstrated for the first time that genetic depletion of *Ythdf1* in murine CRC cells of both MSS and MSI-H could induce accumulation of MDSCs and inhibit the infiltration of T cells in syngeneic CRC mice and humanised mice. On the contrary, intestine-specific *Ythdf1* knockin drives an immunosuppressive TIME that facilitates spontaneous CRC formation. By integrative analyses of methylated RNA immunoprecipitation sequencing (MeRIP-seq), RNA-seq and Ribo-seq, a YTHDF1-m^6A-p65-CXCL1 axis was identified as the mechanism of YTHDF1-induced immunosuppression, leading to the recruitment of MDSCs to suppress effector cells such as functional $CD8^+$ T cells. Moreover, targeting of YTHDF1 by CRISPR or vesicle-like nanoparticles (VNPs)-siRNA enhanced anti-PD1 efficacy in both MSS and MSI-H models, supporting YTHDF1 as a therapeutic target in the immunotherapy of CRC.

METHODS

Clinical samples

Cohort I comprised 206 patients with surgically excised CRC tissues, which derived from Prince of Wales Hospital, Hong Kong. Cohort II was Beijing cohort, consisting of 202 patients with CRC. Paraffinised sample of these two cohorts were used to establish the tissue microarrays (TMA). The clinicopathological features of the two cohorts were provided in online supplemental tables S1and S2. Informed consent was obtained for all patients.

Humanised mouse models

Four-to-five week-old NOD.Cg-Prkdcscid Il2rgtm1Wjl/SzJ (NSG) mice were exposed to total body gamma irradiation (150–170 cGy/animal) and then intravenously injected with 5×10^4 human cord blood-derived $CD34^+$ haematopoietic stem cells (STEMCELL) within 24 hours. The percentage of human CD45 positive cells in $CD34^+$ humanised mice was monitored at weeks 8 and 16 by flow cytometry, after $CD34^+$ haematopoietic stem cells transplantation. $CD34^+$ humanised mice with >20% human $CD45^+$ cells in blood were used for establishment of xenografts. All animal studies followed the guidelines approved by the Animal Experimentation Ethics Committee of The Chinese University of Hong Kong.

Murine CRC models with intestinal-specific *Ythdf1* knockin

Intestinal-specific *Ythdf1* knockin mice (*Ythdf1*$^{loxp/loxp}$*CDX2-cre*) were established. Six to eight weeks old transgenic mice were intraperitoneally injected with tamoxifen (100 mg/kg) to activate *Ythdf1* overexpression. For azoxymethane-dextran sulphate-sodium (AOM/DSS) CRC mice model, 7–8 week-old mice were injected intraperitoneally with AOM (10 mg/kg body weight) (#A5486, Sigma-Aldrich), and the mice were given water containing 1.5% dextran sulfate sodium (DSS) (#9011-18-1, MP Biomedicals) for 4 days, 5 days after AOM injection. The regular drinking water was used for the following 2 weeks. DSS treatment was given for an additional 2 cycles, and the mice were sacrificed on day 80. For *Apc*$^{Min/+}$ CRC mice model, *Ythdf1*$^{loxp/loxp}$*CDX2-cre* mice were crossbred with *Apc*$^{Min/+}$ mice to generate *Apc*$^{Min/+}$ *Ythdf1*$^{loxp/loxp}$*CDX2-cre*, all mice were sacrificed after 16 weeks. All animal experiments in this study were approved by the Animal Experimentation Ethics Committee of CUHK and Xiamen University.

TCGA data analysis

Colorectal adenocarcinoma TCGA data (TCGA, PanCancer Atlas) were acquired from cBioPortal (https://www.cbioportal.org/).[7 8] Coexpression data performed with Spearman's correlation in 526 samples was downloaded also from cBioPortal. Genes correlated with *YTHDF1* in mRNA expression were subjected to gene set enrichment analysis (GSEA_4.1.0).[9] The normalised enrichment scores for IFN-γ signature response was shown. For analysing the association between expression of *YTHDF1* and CXCL1 family members, data from stage IV patients were used. High expression tumour was defined with a z-score higher than 0.7, while low expression with a z-score lower than −0.7. The associations were determined with χ^2 tests.

Statistical analysis

All measurements were acquired using independent samples rather than collected with repeated measurements. GraphPad Prism V.8 (GraphPad Software; San Diego, California) was used for data analysis, and the data were shown as means ± SD, unless stated otherwise. Two-tailed student's t-test was used to conduct statistical analysis, unless stated otherwise. A p value<0.05 was regarded as statistically significant.

Additional methods are provided in the online supplemental material.

RESULTS

YTHDF1 is associated with reduced IFN-γ-related gene signatures and poor prognosis in CRC

By analysing copy number variations of 21 known m^6A regulators using TCGA data, we identified that *YTHDF1* is the top

m^{6}A regulator displaying copy number gain or amplification in nearly 80% of CRC tumours (online supplemental figure S1A). Such an increase of copy number is also concordant with upregulation of mRNA expression (online supplemental figure S1A) and protein expression (online supplemental figure S1C), implicating that YTHDF1 functions in promoting CRC. To establish a link between antitumour immunity and m^{6}A regulators, we then performed GSEA to analyse the correlation between m^{6}A regulators with IFN-γ response gene signature. We found that *YTHDF1* showed a striking negative correlation ($q<0.0001$) with the IFN-γ response pathway (online supplemental figure S1B). Of note, IFN-γ response is associated with the induction of antitumour immunity[10 11] and responsiveness to ICB therapy.[12 13] Consistently, *YTHDF1* expression strongly anticorrelated with an 18 IFN-γ-related gene signature (figure 1A), which predicts anti-PD1 responsiveness in multiple cancer types.[14 15] Furthermore, expression of *CD8A* or CD8$^+$ T cell signature[16] is negatively correlated with *YTHDF1* expression (online supplemental figure S1D). In agreement with TCGA data, IHC staining of TMA from our CRC TMA cohorts showed that high protein expression of YTHDF1 was correlated with low infiltration of CD8$^+$ T cells in cohort I ($p<0.001$, $r=-0.248$, $n=206$) (figure 1B) and cohort II ($p<0.0001$, $r=-0.269$, $n=202$) (figure 1C). These data strongly imply that m^{6}A reader YTHDF1 is associated with impaired antitumour immunity and reduced ICB treatment efficacy.

In agreement with the notion that low CD8$^+$ T cell infiltration is associated with poor prognosis,[17] high expression of YTHDF1 (54.3%, 100/184) predicted poor survival of patients with CRC ($p<0.01$, log-rank test) (online supplemental figure S1E,F). Multivariate Cox regression analysis validated that YTHDF1 was an independent prognostic factor for CRC in cohort II (HR, 1.764; 95% CI 1.058 to 2.939; $p<0.05$) (online supplemental figure S1F). These findings were further verified in cohort I by multivariate Cox regression analysis (online supplemental figure S1E).

Single-cell transcriptomics reveal YTHDF1-induced immunosuppression

To investigate the role of YTHDF1 in regulating antitumour immunity, we used the CRISPR-Cas9 system to knockout *Ythdf1* (*Ythdf1*-KO) in MC38 murine MSI-H CRC cells and injected the cells to syngeneic C57BL6 mice (figure 1D). We found that both tumour volume and weight were reduced by knockout of *Ythdf1* compared with control (NC) (figure 1E). To ask if *Ythdf1*-KO impact TIME, we isolated CD45$^+$ immune cells from the tumours and performed single cell RNA-seq (scRNA-seq) (NC: 1480 cells; *Ythdf1*-KO: 1816 cells). Tumours with *Ythdf1*-KO exhibited strong reduction of granulocytic myeloid-derived suppressor cells (G-MDSCs, cluster 3) and neutrophils compared with NC group (figure 1F and online supplemental figure S2A). In contrast, T cells and NK cells were largely increased in *Ythdf1*-KO tumours (figure 1F and online supplemental figure S2A). We further reclustered T and NK cells into CD4$^+$ T, CD8$^+$ T, NKT and NK cell subsets, and identified that they were simultaneously increased in *Ythdf1*-KO tumours compared with controls (figure 1F). We thus speculated that YTHDF1 can suppress the antitumour immunity through inducing MDSC accumulation. Functional markers of MDSCs, *Il1b*, *Arg2*, *Cxcr2* and *Ccr2* were examined, and these genes were mainly enriched in MDSC clusters (cluster 3 and cluster 4), especially from tumours without *Ythdf1* knockout (figure 1G). Thus, data from this syngeneic model supports an immunosuppressive function of YTHDF1 in CRC.

Ythdf1 knockout reduces MDSCs but increases cytotoxic T cell infiltration

To validate our findings in scRNA-seq analyses, the composition of tumour-infiltrating immune cells in MC38 syngeneic mice was determined by flow cytometry. We confirmed that *Ythdf1* knockout significantly suppressed tumour weight and volume (figure 1C), and flow cytometry revealed that *Ythdf1* knockout decreased MDSCs, but increased CD8$^+$ T and CD4$^+$ T cells in tumours (figure 1H,I). Of MDSCs, G-MDSCs were the predominant subset, and knockout of *Ythdf1* led to the remarkable reduction of G-MDSCs (figure 1I). In line with the immunosuppressive function of MDSCs, we observed significant increase of functional T cells, including IFN-γ$^+$ CD8$^+$ T cells, Granzyme B$^+$ CD8$^+$ T cells, and IFN-γ$^+$ CD4$^+$ T cells in *Ythdf1*-KO group (figure 1H,J).

We next performed the experiment in CT26 (MSS-CRC) with *Ythdf1*-KO to validate the role of YTHDF1 in regulating antitumour immunity. As expected, *Ythdf1*-KO led to reduced tumour volume and weight (figure 2A,B) in CT26 syngeneic mice, together with reduced functional T cells and accumulation of MDSCs (figure 2C,D). Immunofluorescence staining confirmed the decreased infiltration of MDSCs (CD11b$^+$Gr-1$^+$) in both MC38 and CT26 syngeneic tumours on *Ythdf1* knockout (figure 2E and online supplemental figure S2B). Collectively, *Ythdf1* depletion in CRC cells reduced MDSCs and increased functional T cell infiltration. These findings are in line with clinical data demonstrating YTHDF1 anticorrelated with CD8$^+$ T cell and IFN-γ-related signatures (figure 1A–C, online supplemental figureS1B,D).

We asked if the attenuated tumour formation in *Ythdf1*-KO was dependent on CD8$^+$ T cell antitumour immunity. To address this, we depleted CD8$^+$ T cells with an anti-CD8 antibody in the MC38 syngeneic model. Consistent with our hypothesis, depletion of CD8$^+$ T cells restored growth of *Ythdf1*-KO tumours (figure 2F,G), demonstrating that tumour-suppressing function of *Ythdf1*-KO was dependent, at least partially, on CD8$^+$ T cells. This was confirmed in CT26 syngeneic mice showing that anti-CD8 antibody treatment rescued arrested tumour growth in *Ythdf1*-KO group (figure 2H,I). Depletion of CD8$^+$ T cells by anti-CD8 antibody was confirmed by flow cytometry (online supplemental figure S3A,B). Together, *Ythdf1* knockout suppresses CRC growth through the induction of CD8$^+$ T cell-dependent antitumour immunity.

Intestine-specific *Ythdf1* knockin promotes colorectal tumourigenesis and suppresses antitumour immunity in mice

To verify the role of YTHDF1 in spontaneous colorectal tumourigenesis, we generated intestine-specific *Ythdf1* knockin mice (*Ythdf1*$^{loxp/loxp}$*CDX2-cre*) and initiated CRC in these mice by AOM/DSS treatment (figure 3A). We found that the overexpression of *Ythdf1* resulted in increased colon tumour number and size in the AOM/DSS model (figure 3C). Flow cytometry revealed increased MDSC infiltration together with reduced NK, CD4$^+$ T and CD8$^+$ T cells in colon tumours of *Ythdf1* knockin mice compared with wildtype mice (figure 3D). Moreover, we found that *Ythdf1* knockin reduced the proportion of functional T cells as identified by granzyme B, INF-γ and TNF-α expression (figure 3E).

We next sought to validate these results in *Apc*$^{Min/+}$-driven spontaneous CRC (figure 3B) by establishing *Apc*$^{Min/+}$*Ythdf1*$^{loxp/loxp}$*CDX2-cre* mice. Consistently, *Apc*$^{Min/+}$ mice with intestine-specific knockin of *Ythdf1* developed significantly bigger colon tumours than their wild-type littermates (figure 3C). Analysis

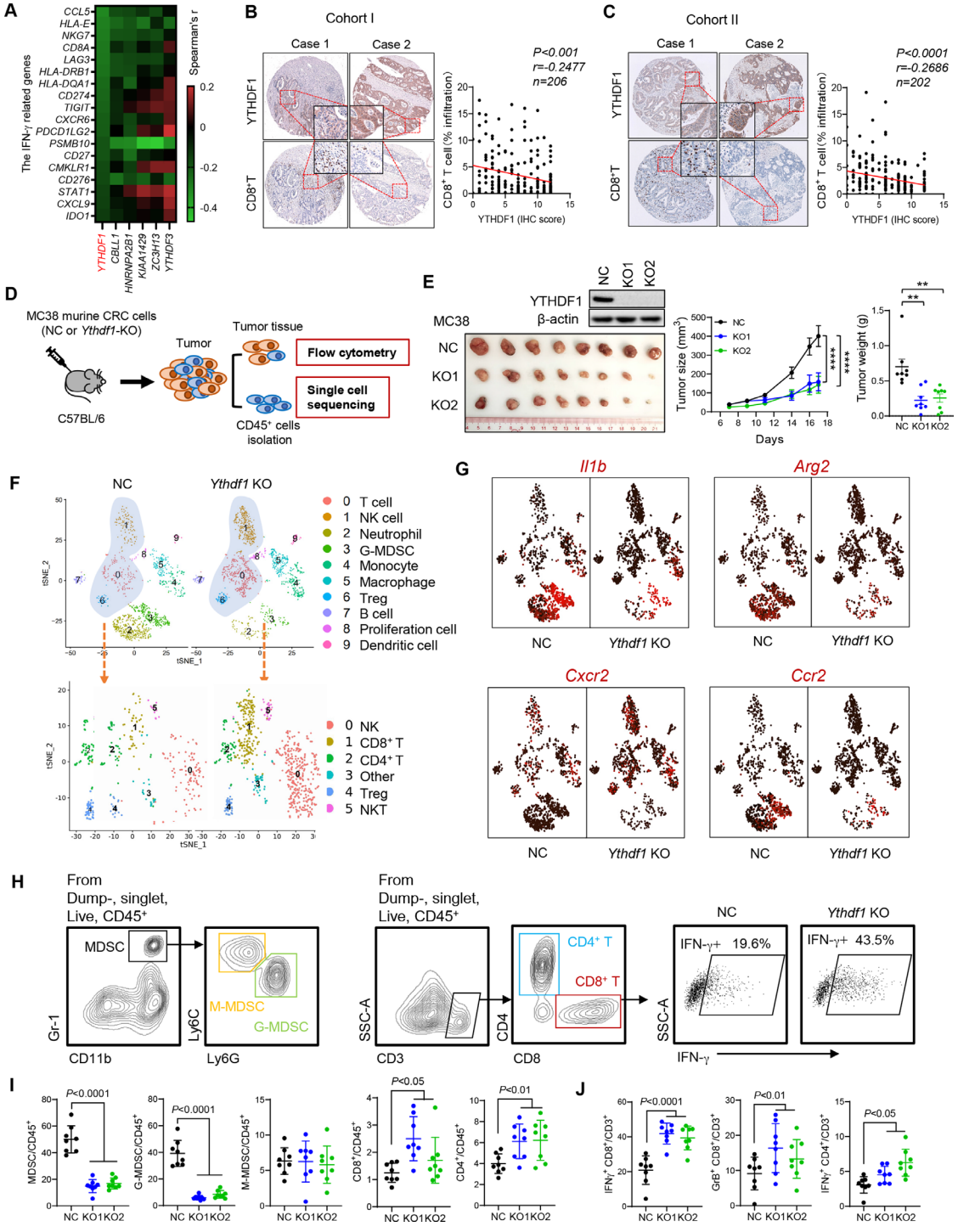

Figure 1 YTH N^6-methyladenosine RNA binding protein 1 (YTHDF1) is associated with an immunosuppressive microenvironment in patients with colorectal cancer (CRC) and its validation by scRNA-seq in immunocompetent mice. (A) Spearman's correlation in mRNA expression between interferon gamma (IFN-γ)-related genes and m^6A regulators in The Cancer Genome Atlas dataset. (B) Correlation between protein levels of YTHDF1 and $CD8^+$ T cell infiltration was determined by immunohistochemistry staining in cohort I (p<0.0001, r=−0.2686, n=202), and (C) validation in cohort II (p<0.001, r=−0.2477, n=206). (D) Experimental design for single-cell analysis of $CD45^+$ cells sorted from the tumours with or without *Ythdf1* by FACS, followed by droplet-enabled scRNA-seq. NC: cells with control sgRNA. *Ythdf1*-KO: cells with CRISPR knockout of *Ythdf1*. (E) Representative image (*left*), tumour volume (*middle*), and weight (*right*) of MC38 syngeneic tumours with or without *Ythdf1* knockout injected in C57BL/6 mice. (F) Upper panel: tSNE plot showing the components of immune cells in MC38 syngeneic tumours with or without *Ythdf1* knockout. Each dot represents a single cell. The same cell type was colour coded. Lower panel: subset analysis of T cell and NK cell clusters shown in tSNE projection regions. (G) Feature plots of characteristic markers of all cell types showing expression levels with low expression in dark red to high expression in bright red. (H) Gating strategies for flow cytometry. Identification of myeloid-derived suppressor cells (MDSC), M-MDSC, and G-MDSC (*left*). Identification of $CD8^+$ T and $CD4^+$ T cells (*middle*). Representative images showing increase of IFN-γ^+ $CD8^+$ T cells in *Ythdf1*-KO tumours in (D) (*Right*). (I) Flow cytometry analysis performed with tumours derived from the indicated cells in (D) (**p<0.01; ****p<0.0001) (linear regression (B, C), two tailed t-test (E, H, I), analysis of variance test (E)). NC: cells with control sgRNA. KO1: cells with *Ythdf1* sgRNA #1. KO2: cells with *Ythdf1* sgRNA #2. GrB: granzyme B.

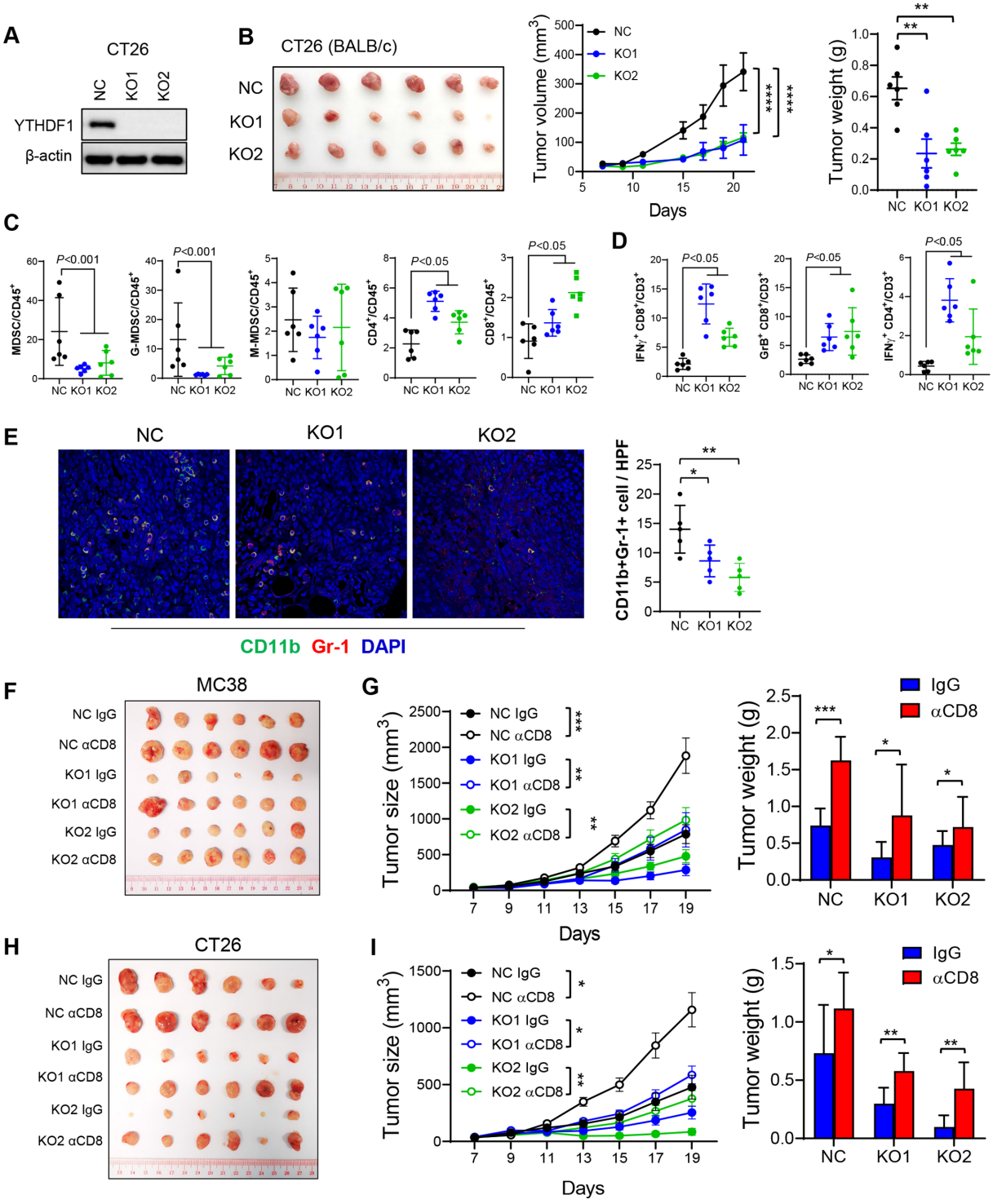

Figure 2 YTH N^6-methyladenosine RNA binding protein 1 (*Ythdf1*) knockout induces antitumour immunity by reduction of myeloid-derived suppressor cell (MDSC) and increase of functional T cells in syngeneic tumours, an effect reversed by $CD8^+$ T cell depletion. (A) Western blot validated *Ythdf1* knockout in CT26 cells. (B) Representative image of CT26 syngeneic tumours with or without *Ythdf1* Knockout (*left*). Knockout of *Ythdf1* in CT26 cells inhibits tumour growth (*middle*) and tumour weight (*right*) in BALB/c mice. (C) MDSC, G-MDSC, M-MDSC, $CD4^+$ T cells and $CD8^+$ T cells from tumours in (B) were analysed by flow cytometry. (D) Flow cytometry analysis assessing the percentage of T cell functional markers interferon gamma (IFN-γ) and granzyme B (GrB) from tumours in (B). (E) Immunofluorescence identifying MDSCs in subcutaneous tumours from BALB/c injected with the indicated CT26 cells (n=5 each group). (F) MC38 NC or *Ythdf1* knockout cells were implanted in C57BL/6 (n=6). Isotype control (IgG) or anti-mouse CD8 antibody (αCD8) were given at 200 µg/mouse on days 4, 7 and 9 post cell injection. Representative images of tumours from each group were shown. (G) Tumour volume (*left*) and weight (*right*) from tumours in (F). (H) CT26 NC or *Ythdf1* knockout cells were implanted in BALB/c (n=6). Isotype control (IgG) or αCD8 were given at 200 µg/mouse on days 4, 7 and 9 post cell injection. Representative images of tumours from each group were shown. (I) Tumour volume (*left*) and weight (*right*) from tumours in (H) (*p<0.05; **p<0.01; ***p<0.001; ****p<0.0001) (two tailed t-test (B, C, D, E, G, H), two-way analysis of variance test (D, G, I)). NC: cells with control sgRNA. KO1: cells with *YTHDF1* sgRNA #1. KO2: cells with *YTHDF1* sgRNA #2.

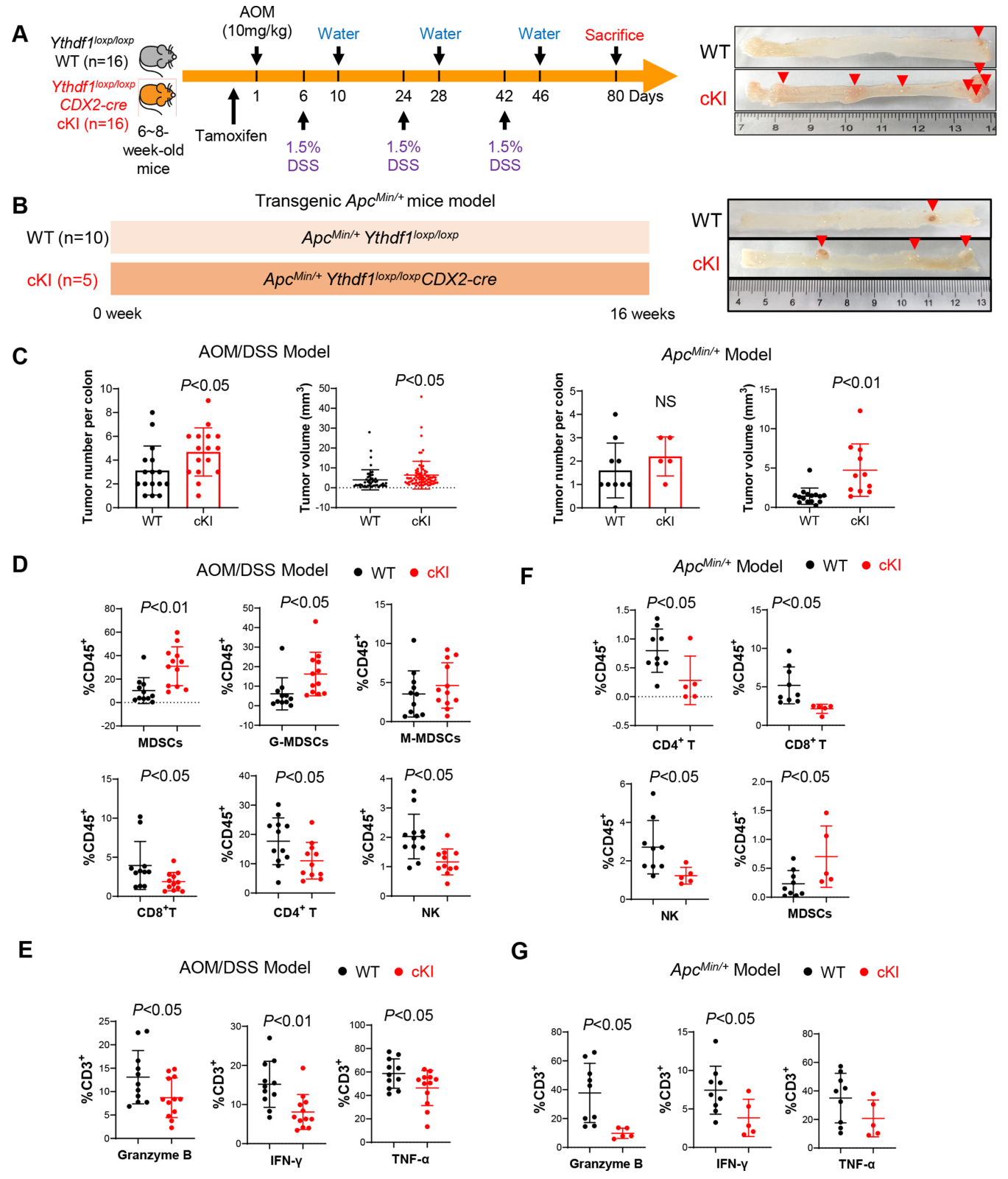

Figure 3 Intestine-specific YTH N^6-methyladenosine RNA binding protein 1 (*Ythdf1*) knockin promotes colorectal tumourigenesis and inhibits antitumour immunity in mice. (A) Scheme for azoxymethane-dextran sulphate-sodium (AOM/DSS) mouse model (*left*). Representative images of the colon at sacrifice (*right*). (B) Scheme for *Apc*$^{Min/+}$ mouse model (*left*). Representative images of the colon at sacrifice (*right*). (C) Tumour number, and tumour size in WT littermates (n=16) and *Ythdf1* Ki mice (n=16) mice treated with AOM-DSS (*left*). Tumour number, and tumour size in *Apc*$^{Min/+}$ *Ythdf1*$^{loxp/loxp}$ (n=10) and *Apc*$^{Min/+}$ *Ythdf1*$^{loxp/loxp}$*CDX2-cre* mice (n=5) mice (*right*). (D) Infiltration of the indicated immune cells in tumours derived from AOM/DSS mice assessed by flow cytometry. (E) Composition of functional T cells in the tumours derived from AOM/DSS mice assessed by flow cytometry. (F) Infiltration of the indicated immune cells in the tumours derived from *Apc*$^{Min/+}$ mice assessed by flow cytometry. (G) Composition of functional T cells in the tumours derived from *Apc*$^{Min/+}$ mice assessed by flow cytometry. Two tailed t-test (C, E, F, G, H). WT: *Ythdf1* wild type; cKI: conditional *Ythdf1* knockin.

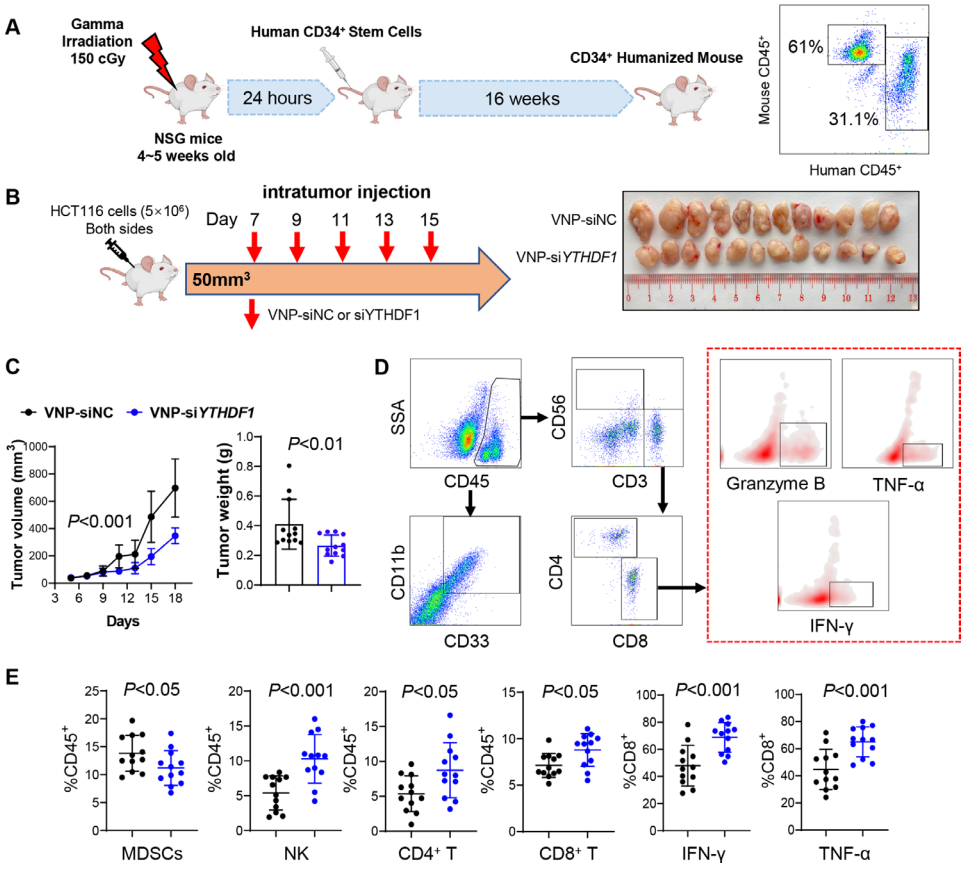

Figure 4 VNP-si*YTHDF1* boosted antitumour immunity in CD34$^+$ humanised mice. (A) Workflow for establishment of CD34$^+$ humanised mice (*left*). Percentage of human CD45$^+$ cells in the CD34$^+$ humanised mice was identified by flow cytometry (*right*). (B) Design for establishment of HCT116 xenografts and treatment with VNP-siNC or VNP-si*YTHDF1* in CD34$^+$ humanised mice (*left*). Representative image of xenografts in different groups (*right*). (C) Tumour volume (*left*) and tumour weight (*right*) in mice in (B). (D) Gating strategies of immune cells in CD34$^+$ humanised mice. (E) Infiltration of CD4$^+$ T, CD8$^+$ T, NK cells, MDSCs and functional CD8 T cells was assessed by flow cytometry in the tumours from (B) (two tailed t-test (C, E), analysis of variance test (C)). VNP, vesicle-like nanoparticles.

of the tumour-infiltrating immune cells demonstrated remarkably decreased infiltration of NK, CD4$^+$ T and CD8$^+$ T cells in tumours with *Apc*^{Min}/+ with knockin of *Ythdf1*, together with the induction of MDSCs (figure 3F). Furthermore, *Ythdf1* knockin reduced granzyme B$^+$, INF-γ$^+$, or TNF-α$^+$ T cells in *Apc*$^{Min/+}$ mice (figure 3G). Collectively, these results support that YTHDF1 fosters an immunosuppressive microenvironment promoting spontaneous CRC.

Targeting YTHDF1 via VNP-si*YTHDF1* boosts antitumour immunity in CD34$^+$ humanised mice

To confirm the role of YTHDF1 in modulating human antitumour immune response, we established the CD34$^+$ humanised mouse model.[18] Mice with peripheral blood mononuclear cells (PBMCs) comprising >20% human CD45$^+$ cells were used (figure 4A). To target YTHDF1 in vivo, we developed VNPs[19] to carry siRNA against *YTHDF1*. The humanised NSG mice bearing human CRC HCT116 xenografts were treated with VNP-siNC or -si*YTHDF1* after tumours reached 50–100 mm^3 (figure 4B). VNP-si*YTHDF1* significantly inhibited tumour volume and weight compared with VNP-siNC (figure 4B,C). We also performed flow cytometry to analyse the TIME (figure 4D). VNP-si*YTHDF1* decreased MDSC infiltration, but increased CD4$^+$ T cell, CD8$^+$ T cell and NK cell accumulation (figure 4E). In addition, more IFN-γ$^+$, TNF-α$^+$ and granzyme B$^+$ CD8$^+$ T cells were identified in tumours receiving VNP-si*YTHDF1* (figure 4E). We also determined the safety of VNP-si*YTHDF1* by measuring serum markers of liver (alanine aminotransferase and aspartate transaminase) and kidney function (creatinine and blood urea nitrogen). Mice treated with VNP-siNC or VNP-si*YTHDF1* did not demonstrate abnormal liver or kidney function indicators (online supplemental figure S4), showing that VNP treatment is well tolerated. Thus, the targeting of YTHDF1 using VNP-si*YTHDF1* is a safe and effective means to enhance antitumour immunity in humanised mice.

YTHDF1 promotes p65 translation to activate TNF/NF-κB signalling

To identify the molecular mechanism by which YTHDF1 elicits immunosuppression, we performed RNA-seq and Ribo-seq in CRC cells with or without knockout of *YTHDF1*. By RNA-seq analysis, differentially expressed genes between MC38-NC and MC38-*YTHDF1*-KO cells were enriched in TNF and NF-κB signalling pathways (online supplemental figure S5A). Consistent result was obtained in another CRC cell line CT26 showing that YTHDF1 regulated TNF/NF-κB signalling pathway (online supplemental figure S5B). In support of these, qPCR validated that *Ythdf1*-KO reduced mRNA expression of TNF/NF-κB targets (online supplemental figure S6A). Furthermore, Ribo-seq data revealed that loss of *YTHDF1* was significantly associated with inactivation of TNF signalling (figure 5A). Accordingly, *YTHDF1* knockout reduced ribosome protected fragment

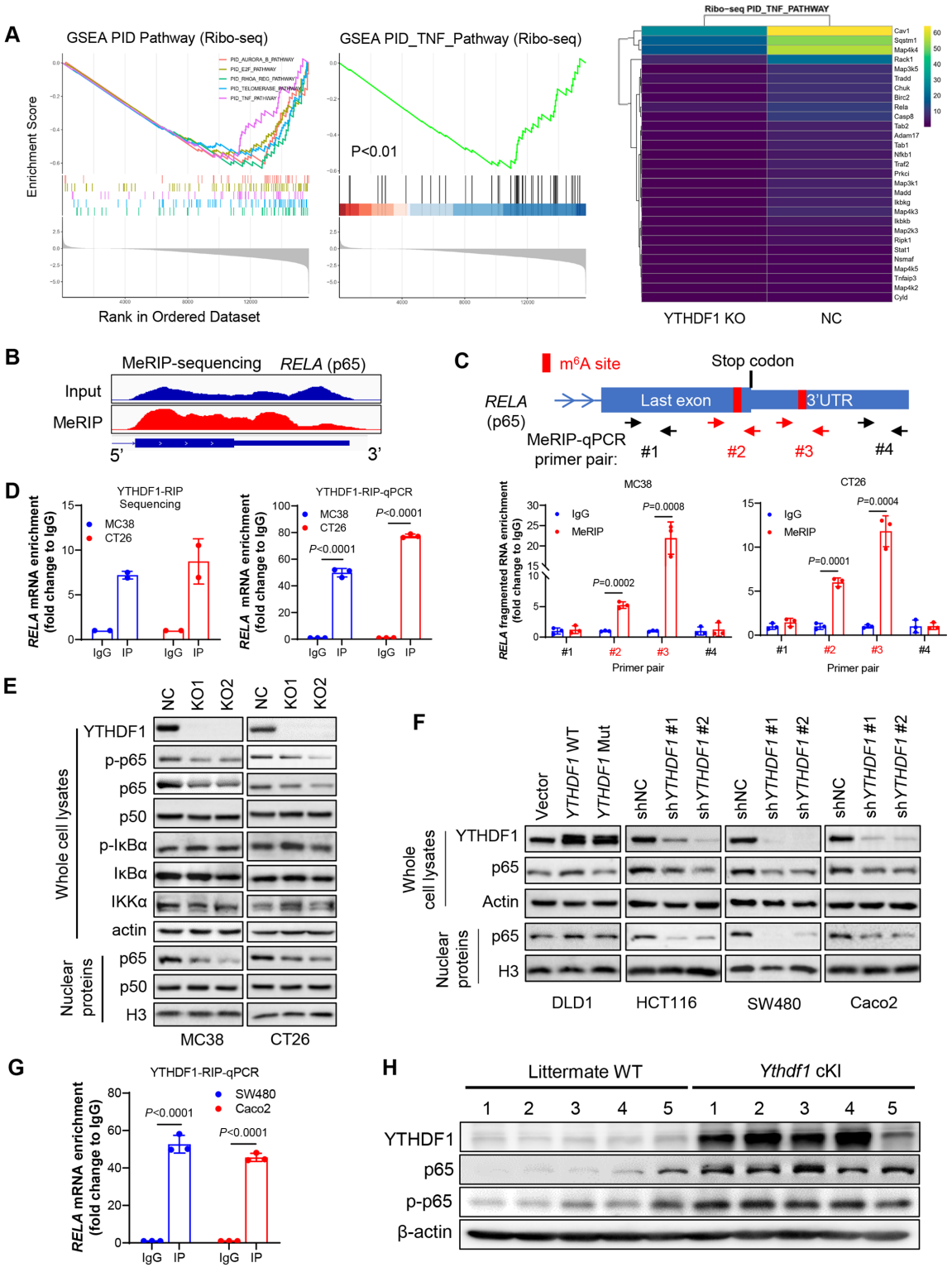

Figure 5 YTH N^6-methyladenosine RNA binding protein 1 (YTHDF1) promotes TNF/NF-kB signalling in CRC through promoting *RELA* (p65) mRNA translation. (A) Differentially expressed genes between CT26 cells with and without knockout of *Ythdf1* were enriched in TNF signalling pathway identifying by Ribo-seq (*left*). Heatmap of genes on TNF signalling pathway (*right*). (B) Methylated RNA immunoprecipitation (MeRIP) sequencing on CT26 cells, showing m^{6}A modifications on last exon or 3'UTR of *RELA* (p65) mRNA. (C) Scheme showing the design of primers for MeRIP-qPCR to validate m^{6}A modifications on p65 mRNA. Potential m^{6}A sites were highlighted in red (*upper*). MeRIP-qPCR primers are indicated by arrows. MeRIP-qPCR validated m^{6}A modification with primers #2 and #3 (lower). (D) RNA immunoprecipitation sequencing with anti-YTHDF1 antibody (YTHDF1-RIP) showing the enrichment of p65 mRNA compared with IgG control (*left*). YTHDF1-RIP-qPCR with primers specific to murine p65 mRNA (*right*). (E) Western blot of key effectors of TNF/NF-κB signalling pathway on knockout of *Ythdf1*. (F) Western blot analysis performed with indicated human CRC cells overexpressing wild-type (WT) or mutant (mut) *YTHDF1*, or *YTHDF1* knockdown with shRNA. Non-targeted shRNA (shNC) were used as control. (G) YTHDF1-RIP-qPCR with primers specific to human p65 mRNA. (H) Expression of p65 and phospho-p65 was determined by western blot in colon tumours from the intestine-specific *Ythdf1* knockin mice and wildtype littermates. cKI: conditional knockin (two tailed t-test (C, D, G)).

abundance of genes involved in TNF signalling (figure 5A). Thus, YTHDF1 could regulate TNF/NF-κB signalling by promoting protein translation. Since YTHDF1 functions as a m^6A reader, we next performed m^6A immunoprecipitation sequencing (MeRIP-seq) to pinpoint m^6A-modified transcripts. By screening m^6A peaks in mRNAs involved in TNF signalling, we identified two m^6A sites close to the stop codon of p65 mRNA (figure 5B), which was validated by MeRIP-qPCR (figure 5C). Importantly, we identified a direct interaction between YTHDF1 and p65 mRNA by RNA immunoprecipitation (RIP) sequencing and RIP-qPCR with anti-YTHDF1 antibody (figure 5D). Thus, p65 mRNA is a direct target of YTHDF1. We found that knockout of *Ythdf1* attenuated p65 protein expression, especially nuclear p65 expression, in both CT26 and MC38 cells, without affecting the expression of other regulators of NF-κB pathways such as IKKα and IκBα (figure 5E). Notably, mRNA expression of p65 was unchanged in *Ythdf1*-KO cells (online supplemental figure S6B), supporting that YTHDF1 regulates p65 primarily at the level of protein translation, which is in line with the reported YTHDF1 function of facilitating translation of its targets. Consistent results were obtained in human CRC cells showing that overexpression of wild-type *YTHDF1*, but not dysfunctional mutant,[5 6] elevated p65 protein expression; conversely, *YTHDF1* knockdown attenuated p65 protein in human CRC cells (figure 5F). RIP-qPCR using anti-YTHDF1 antibody also confirmed a direct interaction between YTHDF1 and p65 mRNA in human CRC cells (figure 5G). We next sought to validate the association of YTHDF1 and p65 in vivo. In *Ythdf1* knockin mice, both p65 and phospho-p65 protein were increased in colon tumours (figure 5H). Collectively, YTHDF1 promotes p65 protein expression to activate TNF and NF-κB signalling in vitro and in vivo.

YTHDF1 promotes MDSC migration via p65-CXCL1 axis

To understand the link between YTHDF1-induced p65 and its immunosuppression, we performed a cytokine multiplex immunoassay for the detection of 23 different mouse cytokines in conditioned medium of CRC cells, tumour lysates, and serum from mice bearing syngeneic tumours. Among these cytokines, CXCL1 was consistently reduced by *Ythdf1*-KO (figure 6A), and this reduction of CXCL1 was confirmed by ELISA assay (figure 6B). CXCL1 has been reported as a transcriptional target of NF-κB signalling,[20 21] and it promotes MDSC chemotaxis via interaction with its receptor CXCR2.[22–24] Given that *Ythdf1*-KO reduced MDSC infiltration in CRC TIME, we asked whether YTHDF1 modulates MDSC migration. As such, in vitro MDSC migration assay was conducted. We found that conditioned medium from wild-type CRC cells enhanced MDSC migration, which was impaired by the knockout of *Ythdf1* (figure 6C). Blocking CXCL1-CXCR2 interaction by CXCR2 inhibitor SB265610 eliminated the difference between control and *Ythdf1*-KO culture supernatant in mediating MDSC migration (figure 6C). Thus, YTHDF1 promotes MDSC migration through CXCL1/CXCR2 axis. We next asked whether YTHDF1 could regulate *Cxcl1* mRNA expression. As expected, *Ythdf1* knockout significantly inhibited *Cxcl1* mRNA levels in murine (figure 6D) and human CRC cell lines (online supplemental figure S7A). Conversely, the overexpression of wild-type *YTHDF1*, but not its dysfunctional mutant, elevated *CXCL1* transcription and protein levels in human CRC cells (online supplemental figure S7A). NF-κB activators, such as TNF-α and IL-1β, have been reported to induce *CXCL1* expression.[25] We thus treated MC38 cells with TNF-α and measured CXCL1 mRNA and secretion. TNF-α stimulated *Cxcl1* mRNA and secretion, an effect abrogated by the loss of *Ythdf1* (online supplemental figure S7B). To confirm the link between YTHDF1 and CXCL1 in human CRC, we examined the association between *YTHDF1* and *CXCL1* expression in TCGA CRC cohort. Consistently, *YTHDF1*-high CRC demonstrated high *CXCL1* expression (online supplemental figure S7C). Besides *CXCL1*, *CXCL2* also positively correlated with *YTHDF1* (online supplemental figure S7C). In contrast, *CXCL5* and *CXCL8* expression negatively correlated with *YTHDF1* (online supplemental figure S7C). Considering the role of YTHDF1 in promoting MSDC infiltration, we next performed CRC TMA of CD33, a marker for G-MDSCs.[26 27] We found that YTHDF1 protein levels positively correlated with the proportion of intratumoural $CD33^+$ cells (online supplemental figure S8). Our findings thus support a YTHDF1-p65-CXCL1/CXCR2 axis mediating MDSC migration in CRC.

We next investigated if YTHDF1 affects MDSC function. $CD11b^+Gr\text{-}1^+$ MDSCs were isolated from MC38 syngeneic tumours and then cocultured with T cells in vitro (figure 6E). MDSCs isolated from control tumours suppressed T cell proliferation; however, MDSCs from *Ythdf1*-KO tumours exhibited significantly less suppressive activity against the proliferation of both $CD8^+$ T cells and $CD4^+$ T cells compared with MDSCs from the control (figure 6F,G). In support of this, MDSCs isolated from *Ythdf1*-KO tumours have reduced expression of MDSC functional markers *Nos2*, *Arg1*, and *Cd274* compared with *Ythdf1*-WT tumours (online supplemental figure S9A). Flow cytometry confirmed that $iNOS^+$ MDSCs was attenuated *Ythdf1*-KO tumours (online supplemental figure S9B). These data validate the reported immunosuppressive function of MDSCs on key effector cells, including $CD8^+$ T cells and $CD4^+$ T cells,[28] and support that *YTHDF1*-expressing CRC recruits functional MDSCs.

YTHDF1 is a potential therapeutic target for CRC immunotherapy

Considering that reduced infiltration of MDSCs has been reported to correlate with enhanced immunotherapeutic efficacy in various cancer types,[22 29 30] we sought to test if targeting YTHDF1 augments anti-PD1 therapy in CRC. As expected, we found that knockout of *Ythdf1* boosted efficacy of anti-PD1 in MC38 (MSI-H) syngeneic tumours and prolonged survival of the tumour-bearing mice (figure 7A). We further exploited the VNPs system to deliver specific *Ythdf1*-siRNA into tumours. When MC38 syngeneic tumours reached 50∼100 mm^3, we treated the mice with VNP-si*Ythdf1* (or VNP-siNC) and anti-PD1 treatment (or IgG). VNP-si*Ythdf1* significantly suppressed MC38 tumour growth compared with VNP-siNC (figure 7B,C). Remarkably, the combination of VNP-si*Ythdf1* plus anti-PD1 exerted the strongest inhibitory effect against tumour growth (figure 7B,C).

We further addressed if targeting YTHDF1 can overcome anti-PD1 resistance in MSS CRC based on syngeneic CT26 (MSS CRC) tumour model. CT26 cells with *Ythdf1* knockout were thus injected to the syngeneic mice and treated with anti-PD1. We found that knockout of *Ythdf1* significantly enhanced anti-PD1 treatment efficacy in CT26 syngeneic tumours, which otherwise were non-responsive to ICB therapy (figure 7D,E).

Flow cytometry analysis further revealed that combination of *Ythdf1* silencing and anti-PD1 remarkably increased tumour-infiltrating functional $CD8^+$ T cells, including IFN-γ^+ $CD8^+$ T cells and Granzyme B^+ $CD8^+$ T cells in both CT26 and MC38 syngeneic models (figure 7F,G). Furthermore, combinational treatment strongly reduced accumulation of MDSCs, whereas

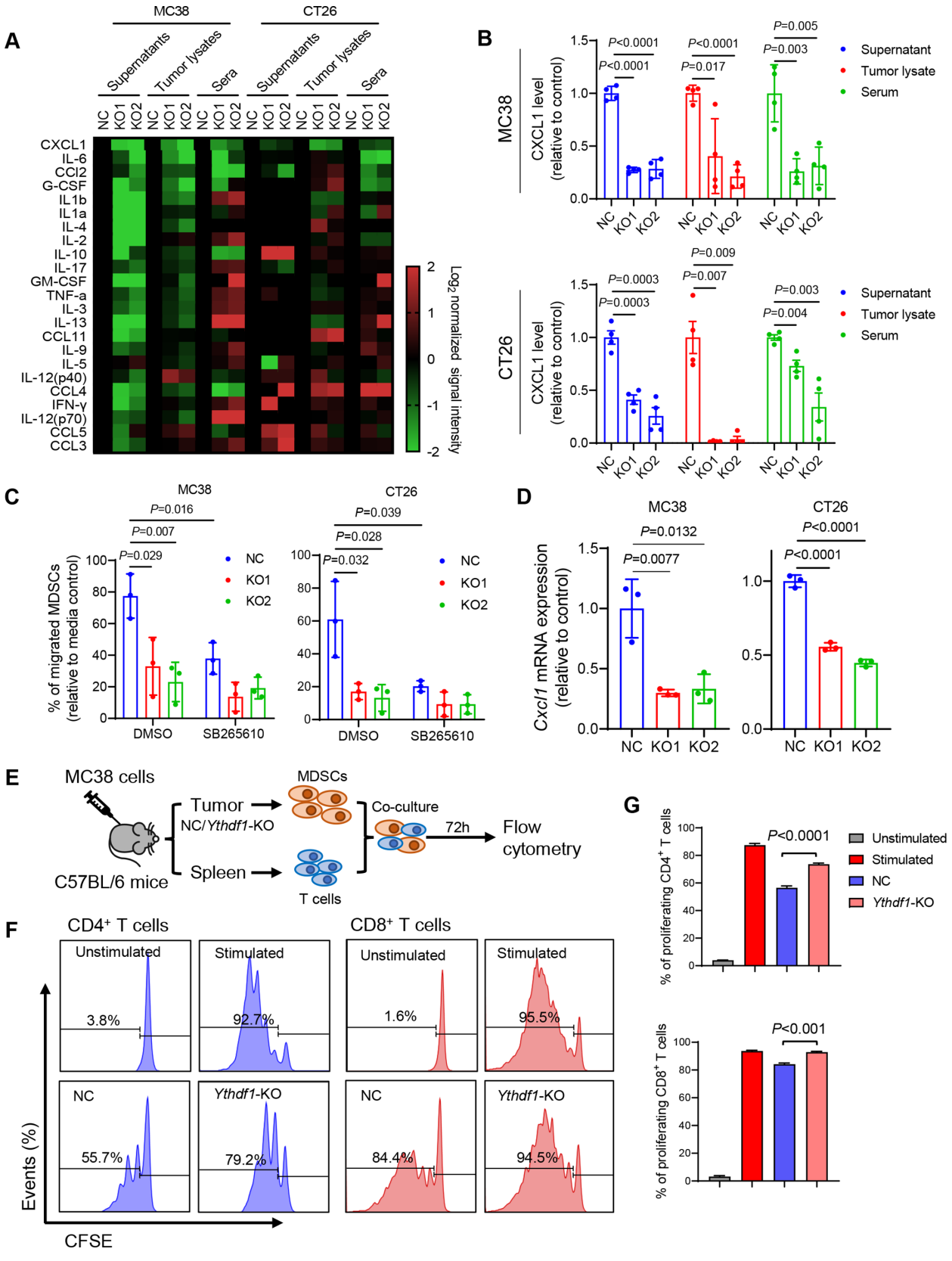

Figure 6 Loss of YTH N^6-methyladenosine RNA binding protein 1 (*Ythdf1*) promotes reduction of myeloid-derived suppressor cells (MDSCs) by decreasing CXCL1 secretion. (A) Multiplex mouse cytokine immunoassay assessing levels of 23 cytokines in cell culture supernatants from MC38 and CT26 cell culture, and tumour lysates and sera from MC38 and CT26 syngeneic tumour models. (B) ELISA validation of levels of CXCL1 in the indicated materials as in (A) (n=4 each group). (C) MDSC migration was assessed in vitro with transwell migration assay using conditional medium derived from the indicated cells. CXCR2 inhibitor SB265610 was used at 5 µM. (D) RT-qPCR determination of *Cxcl1* mRNA expression in the indicated cells. (E) Flow chart of T cell suppression assay. (F) Representative images of flow cytometry assessing the proliferation of CFSE-labelled T cells cocultured with MDSCs isolated as (E). (G) Quantification of (F) (two tailed t-test (C, D, E, G)).

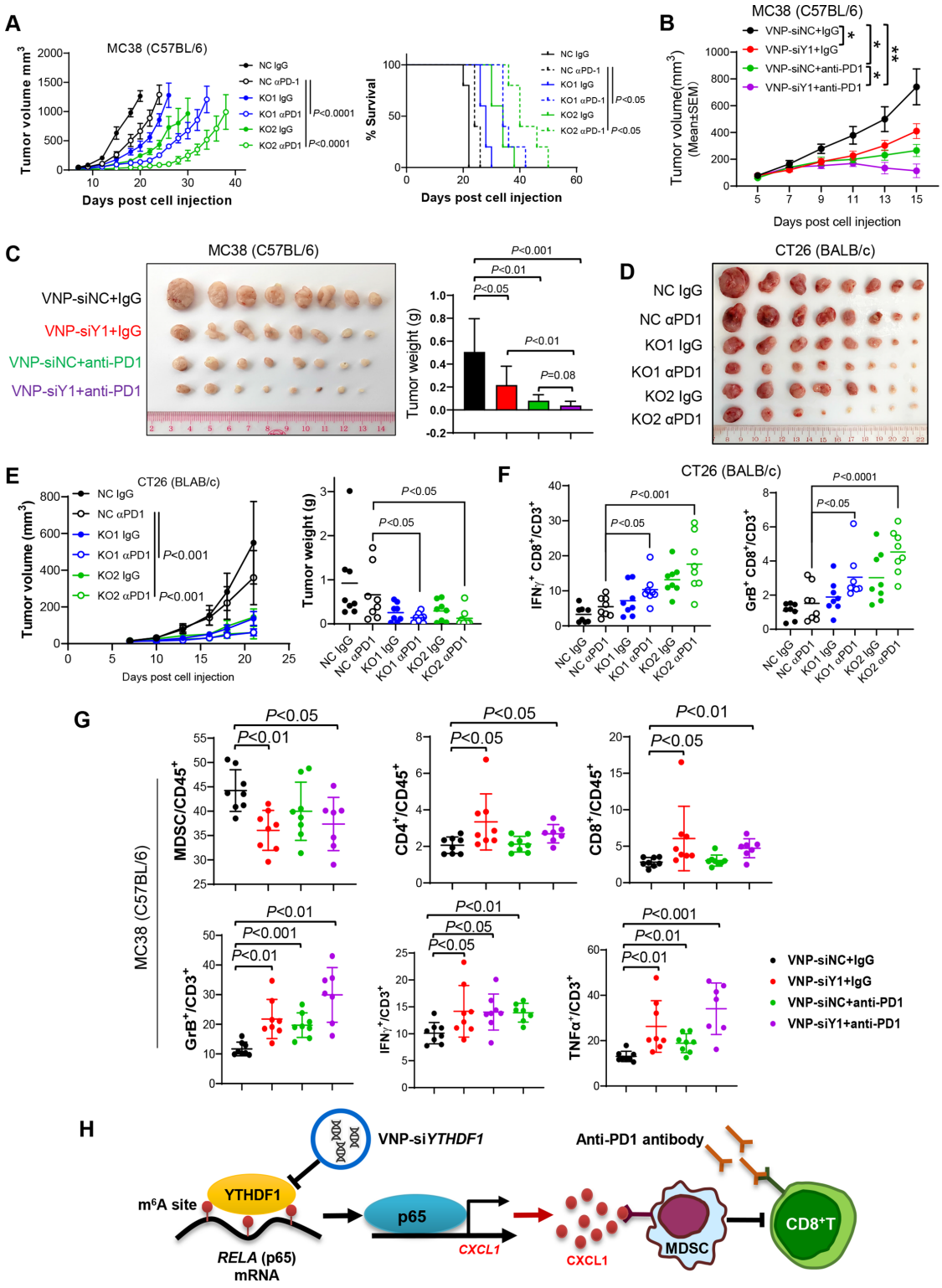

Figure 7 Targeting YTH N^6-methyladenosine RNA binding protein 1 (*YTHDF1*) augmented anti-PD1 blockade therapy in both microsatellite instability-high (MSI-H) and microsatellite stable colorectal cancer (CRC). (A) MC38 cells with or without *Ythdf1* knockout were implanted into C57BL/6 mice and treated with IgG or anti-PD1 (αPD1; n=5 per group). Tumour volume (*left*) and mice survival (*right*) were presented. Euthanasia was applied when tumour burden was greater than or equal to 1500 mm^3 or when the mouse was moribund. (B) Growth curve of subcutaneous tumours from C57BL/6 injected with MC38 and treated with the indicated treatments. Vesicle-like nanoparticle (VNP)-siRNAs were given intratumorally. And αPD1 was given with intraperitoneal injection. (C) Images and weight of the tumours from (B). (D) The indicated CT26 cells were subcutaneously injected in BALB/c mice. The mice were treated with control or αPD1 (n=8 each group). Tumours removed from the mice at sacrifice were shown. (E) Tumour growth curve (*left*) and tumour weight (*right*) in (D). (F) Flow cytometry performed with the tumours in (D). (G) Top panel: flow cytometry assessing the proportion of MDSCs, CD4$^+$ T cells, and CD8$^+$ T cells in total CD45$^+$ cells in tumours in (B). Lower panel: flow cytometry assessing functional CD8$^+$ T cells in tumours in (B). (H) Schematic of the m^{6}A-YTHDF1-p65-CXCL1 axis inducing MDSC accumulation and hence suppressing T cell function in CRC (two tailed t-test (C, D, F, G, H); analysis of variance test (A, C, F); long-rank test (A)). siY1: si*YTHDF1*. GrB: granzyme B.

$CD4^+$ T cells and $CD8^+$ T cells were induced (figure 7G). Thus, targeting of YTHDF1 not only potentiates ICB therapeutic efficacy in MSI-H CRC, but also overcomes ICB resistance in MSS CRC by suppressing recruitment of MDSCs and improving functionality of $CD8^+$ T cells.

DISCUSSION

YTHDF1 is a m^6A reader is frequently upregulated in CRC, but its role in antitumour immunity is largely unknown. Here, our study demonstrates for the first time that high YTHDF1 expression in CRC drives immunosuppression. Single-cell profiling reveals that YTHDF1 is crucial to the recruitment of MDSCs, which in turn attenuated T cell infiltration and function in CRC. This phenomenon is consistently found in syngeneic tumours, intestine-specific *YTHDF1* knockin mice and $CD34^+$ humanised mice. Taken together, our data demonstrate that YTHDF1 promotes an immunosuppressive tumour microenvironment to facilitate CRC tumourigenesis.

A series of in vivo models validated the role of YTHDF1 in recruitment of MDSCs in CRC. In CRC syngeneic models, *Ythdf1* knockout inhibited MDSC accumulation. Conversely, intestine-specific *Ythdf1* knockin accelerated colorectal tumourigenesis in AOM/DSS and $Apc^{Min/+}$ models, concomitant with increased intratumoural MDSCs. Moreover, *YTHDF1* silencing also impaired infiltration of human MDSCs in $CD34^+$ humanised mice. MDSCs are a highly diverse population of immature myeloid cells, including granulocytic MDSCs and monocytic MDSCs. Both of them, especially G-MDSCs, possess potent immunosuppressive activity.[31] In vitro MDSC migration assays directly validated that YTHDF1 plays a crucial role in MDSC chemotaxis. Our results support that YTHDF1 promotes colorectal tumourigenesis via MDSC-mediated immunosuppression.

MDSCs primarily exert their immunosuppressive effect by inhibiting key effector cell proliferation and activation.[28] Indeed, we found that *Ythdf1* knockout induces infiltration of $CD4^+$ T-cells, $CD8^+$ T cells and NK cells in CRC tumours and $CD34^+$ humanised mice, with increased expression of cytotoxic markers granzyme B, INF-γ and TNF-α whereas intestine-specific *Ythdf1* knockin correlated with dampened infiltration and activity status of these effector cells. In vitro studies also demonstrated that MDSCs isolated from *Ythdf1*-null tumours have impaired capacity to suppress T cell proliferation. Together, our data support that YTHDF1-driven functional MDSC accumulation exerts an inhibitory effect on antitumour immune cells to promote immune evasion in CRC.

We next deciphered the molecular basis of YTHDF1-driven MDSC accumulation in CRC. As YTHDF1 functions as a m^6A reader, we performed integrative RNA-seq, Ribo-seq and MeRIP-seq to identify candidate targets of YTHDF1 in CRC. Although several signalling pathways were identified in MSS (CT26) and MSI-H (MC38) CRC, TNF/NF-κB signalling pathway is the top pathway commonly induced by YTHDF1 in both models. We further unravelled p65 subunit of NF-κB as a direct target of YTHDF1. YTHDF1, but not its dysfunctional mutant, binds to m^6A-modified p65 mRNA to increase p65 protein levels without affecting its mRNA expression, implying that YTHDF1 promotes p65 translation in m^6A-dependent manner. TNF/NF-κB signalling is often activated in tumour cells, and induces expression of proinflammatory genes encoding cytokines and chemokines.[32] By cytokine profiling, we found that CXCL1 mRNA expression and secretion were unanimously repressed by genetic inhibition of *Ythdf1* in mouse and human CRC cell lines, syngeneic mice and transgenic mice. CXCL1 plays a pivotal role in promoting MDSCs chemotaxis in TIME via interaction with CXCR2.[33] In line with this, we found that YTHDF1 mediates the migration of MDSCs via a CXCL1-CXCR2 axis, an effect abolished by an CXCR2 inhibitor. Together, YTHDF1-mediated p65 signalling promotes MDSCs via CXCL1 secretion. Apart from CXCL1, alternative NF-κB downstream targets were also down-regulated by *Ythdf1* knockout. It will be of interest to further explore the collateral impact of YTHDF1 on NF-κB-dependent expression of cytokines and chemokines on the immunosuppressive TIME of CRC.

MDSCs have been reported to exert immunosuppressive function on key effector cells, including $CD8^+$ T cells, $CD4^+$ T cells and NK cells.[28] MDSCs exert their antagonistic effect on antitumour T cells via a myriad of mechanisms, including depletion of intratumoural arginine via Arginase-1, induction of oxidative stress via iNOS, and secretion of immunosuppressive molecules such as TGF-β.[31] Here, we showed that depleting *Ythdf1* in cancer cells suppressed intratumoural MDSCs and mitigated the immunosuppressive function of MDSCs on effector cells. MDSCs and T cell coculture studies demonstrated that MDSCs from *Ythdf1*-KO tumours have impaired capacity to suppress the cell proliferation of both $CD8^+$ T cells and CD4 T^+ cells when compared with control tumours. Our findings thus support that YTHDF1 mediates the recruitment of functional MSDCs, which inhibit the function and proliferation of effector T cells in CRC, leading to compromised immune surveillance (figure 7H).

In the clinic, ICI therapy only shows beneficial effects to a small proportion of patients with MMR or MSI-H metastatic CRC, whereas the majority of CRCs with MSS status are largely non-responsive.[34] This can be partially attributed to presence of MDSCs and the formation of immunosuppressive tumour microenvironment. Given that knockout of *Ythdf1* reduced MDSC infiltration in CRC tissues to revert immune suppression, we thus explored therapeutic implications of targeting YTHDF1 in both MC38 (MSI-H) and CT26 (MSS) syngeneic CRC models. *Ythdf1* silencing boosted the anti-PD1 efficacy in MC38 syngeneic model. More importantly, targeting of YTHDF1 reversed anti-PD1 resistance in CT26 (MSS) syngeneic model, highlighting the broad utility of YTHDF1-targeting approach in promoting ICB efficacy not only in MSI-H CRC, but also MSS CRC that otherwise is resistant to ICB therapy.

As there is no currently available drug for YTHDF1, here we developed a nanoparticle-based delivery system[35] to deliver *YTHDF1*-siRNA in vivo. In syngeneic mouse models and humanised mice models of CRC, we observed the robust effect of VNP-si*YTHDF1* that remarkably elevated the infiltration of functional T cells and enhanced tumour response to anti-PD1 therapy. Targeting of YTHDF1 thus represents a promising immunotherapeutic target in CRC.

In conclusion, YTHDF1 expression in CRC recruits immunosuppressive MDSCs via activating m^6A-p65-CXCL1 axis to inhibit T cells, thereby promoting CRC. Targeting YTHDF1 plus anti-PD1 therapy demonstrates promising antitumour efficacy against CRC, corroborating that YTHDF1 is a potential therapeutic target for CRC.

Contributors YB and JZ performed the experiments, analysed the data and drafted the manuscript. HC and CCW commented on the study and revised the paper. CL performed animal experiments. YD and DH performed bioinformatics analyses. HG, DC and YP performed experiments. WK and KFT performed histological staining and evaluation. JY designed and supervised the study and revised the manuscript. JY acts as the guarantor of the study.

Funding This study was supported by RGC Collaborative Research Fund (C4039-19GF), National Natural Science Foundation of China (81972576), RGC-GRF

(14110819, 14111621), RGC Research Impact Fund Hong Kong (R4032-21F), Vice-Chancellor's Discretionary Fund CUHK.

Competing interests None declared.

Patient and public involvement Patients and/or the public were not involved in the design, or conduct, or reporting, or dissemination plans of this research.

Patient consent for publication Not applicable.

Ethics approval This study was approved by Clinical Research Ethics Committee of the Chinese University of Hong Kong and Beijing Caner Hospital.

Provenance and peer review Not commissioned; externally peer reviewed.

Data availability statement Data are available upon reasonable request.

ORCID iDs
Huarong Chen http://orcid.org/0000-0003-2192-1864
Wei Kang http://orcid.org/0000-0002-4651-677X
Jun Yu http://orcid.org/0000-0001-5008-2153

REFERENCES

1 Biller LH, Schrag D. Diagnosis and treatment of metastatic colorectal cancer: a review. *JAMA* 2021;325:669–85.
2 André T, Shiu K-K, Kim TW, *et al*. Pembrolizumab in microsatellite-instability-high advanced colorectal cancer. *N Engl J Med* 2020;383:2207–18.
3 Delaunay S, Frye M. Rna modifications regulating cell fate in cancer. *Nat Cell Biol* 2019;21:552–9.
4 Lin X, Chai G, Wu Y, *et al*. RNA m^6a methylation regulates the epithelial mesenchymal transition of cancer cells and translation of snail. *Nat Commun* 2019;10:2065.
5 Pi J, Wang W, Ji M, *et al*. YTHDF1 promotes gastric carcinogenesis by controlling translation of FZD7 *Cancer Res* 2021;81:2651–65.
6 Liu T, Wei Q, Jin J, *et al*. The M6a reader YTHDF1 promotes ovarian cancer progression via augmenting eIF3c translation. *Nucleic Acids Res* 2020;48:3816–31.
7 Cerami E, Gao J, Dogrusoz U, *et al*. The cbio cancer genomics portal: an open platform for exploring multidimensional cancer genomics data. *Cancer Discov* 2012;2:401–4.
8 Gao J, Aksoy BA, Dogrusoz U, *et al*. Integrative analysis of complex cancer genomics and clinical profiles using the cbioportal. *Sci Signal* 2013;6:pl1.
9 Subramanian A, Tamayo P, Mootha VK, *et al*. Gene set enrichment analysis: a knowledge-based approach for interpreting genome-wide expression profiles. *Proc Natl Acad Sci U S A* 2005;102:15545–50.
10 Tigano M, Vargas DC, Tremblay-Belzile S, *et al*. Nuclear sensing of breaks in mitochondrial DNA enhances immune surveillance. *Nature* 2021;591:477–81.
11 Sun L, Kees T, Almeida AS, *et al*. Activating a collaborative innate-adaptive immune response to control metastasis. *Cancer Cell* 2021;39:1361–74.
12 Gao J, Shi LZ, Zhao H, *et al*. Loss of IFN-γ pathway genes in tumor cells as a mechanism of resistance to anti-CTLA-4 therapy. *Cell* 2016;167:397–404.
13 Sharma P, Hu-Lieskovan S, Wargo JA, *et al*. Primary, adaptive, and acquired resistance to cancer immunotherapy. *Cell* 2017;168:707–23.
14 Ayers M, Lunceford J, Nebozhyn M, *et al*. IFN-γ-related mrna profile predicts clinical response to PD-1 blockade. *J Clin Invest* 2017;127:2930–40.
15 Cristescu R, Mogg R, Ayers M, *et al*. Pan-tumor genomic biomarkers for PD-1 checkpoint blockade-based immunotherapy. *Science* 2018;362:eaar3593.
16 Wang W, Green M, Choi JE, *et al*. Cd8+ T cells regulate tumour ferroptosis during cancer immunotherapy. *Nature* 2019;569:270–4.
17 Pagès F, Mlecnik B, Marliot F, *et al*. International validation of the consensus immunoscore for the classification of colon cancer: a prognostic and accuracy study. *Lancet* 2018;391:2128–39.
18 Choi Y, Lee S, Kim K, *et al*. Studying cancer immunotherapy using patient-derived xenografts (pdxs) in humanized mice. *Exp Mol Med* 2018;50:99.
19 Rezvantalab S, Drude NI, Moraveji MK, *et al*. PLGA-based nanoparticles in cancer treatment. *Front Pharmacol* 2018;9:1260.
20 Scortegagna M, Cataisson C, Martin RJ, *et al*. Hif-1Alpha regulates epithelial inflammation by cell autonomous NFkappaB activation and paracrine stromal remodeling. *Blood* 2008;111:3343–54.
21 Kemp SB, Carpenter ES, Steele NG, *et al*. Apolipoprotein E promotes immune suppression in pancreatic cancer through NF-κB-mediated production of CXCL1. *Cancer Res* 2021;81:4305–18.
22 Highfill SL, Cui Y, Giles AJ, *et al*. Disruption of CXCR2-mediated MDSC tumor trafficking enhances anti-PD1 efficacy. *Sci Transl Med* 2014;6:237ra67.
23 Wang D, Sun H, Wei J, *et al*. Cxcl1 is critical for premetastatic niche formation and metastasis in colorectal cancer. *Cancer Res* 2017;77:3655–65.
24 Zhang Q, Ma C, Duan Y, *et al*. Gut microbiome directs hepatocytes to recruit mdscs and promote cholangiocarcinoma. *Cancer Discov* 2021;11:1248–67.
25 Olivera I, Sanz-Pamplona R, Bolaños E, *et al*. A therapeutically actionable protumoral axis of cytokines involving IL-8, TNFα, and IL-1β. *Cancer Discov* 2022;12:2140–57.
26 Bronte V, Brandau S, Chen S-H, *et al*. Recommendations for myeloid-derived suppressor cell nomenclature and characterization standards. *Nat Commun* 2016;7:12150.
27 Cassetta L, Baekkevold ES, Brandau S, *et al*. Deciphering myeloid-derived suppressor cells: isolation and markers in humans, mice and non-human primates. *Cancer Immunol Immunother* 2019;68:687–97.
28 Veglia F, Sanseviero E, Gabrilovich DI. Myeloid-Derived suppressor cells in the era of increasing myeloid cell diversity. *Nat Rev Immunol* 2021;21:485–98.
29 Steele CW, Karim SA, Leach JDG, *et al*. CXCR2 inhibition profoundly suppresses metastases and augments immunotherapy in pancreatic ductal adenocarcinoma. *Cancer Cell* 2016;29:832–45.
30 Greene S, Robbins Y, Mydlarz WK, *et al*. Inhibition of MDSC trafficking with SX-682, a CXCR1/2 inhibitor, enhances NK-cell immunotherapy in head and neck cancer models. *Clin Cancer Res* 2020;26:1420–31.
31 Gabrilovich DI, Nagaraj S. Myeloid-Derived suppressor cells as regulators of the immune system. *Nat Rev Immunol* 2009;9:162–74.
32 Hoesel B, Schmid JA. The complexity of NF-κB signaling in inflammation and cancer. *Mol Cancer* 2013;12:86.
33 Kumar V, Patel S, Tcyganov E, *et al*. The nature of myeloid-derived suppressor cells in the tumor microenvironment. *Trends Immunol* 2016;37:208–20.
34 Overman MJ, Lonardi S, Wong KYM, *et al*. Durable clinical benefit with nivolumab plus ipilimumab in DNA mismatch repair-deficient/microsatellite instability-high metastatic colorectal cancer. *J Clin Oncol* 2018;36:773–9.
35 Mitchell MJ, Billingsley MM, Haley RM, *et al*. Engineering precision nanoparticles for drug delivery. *Nat Rev Drug Discov* 2021;20:101–24.

Supplementary Methods:

Cell lines

CT26 (CRL-2638), DLD1 (CCL-221), HCT116 (CCL-247), SW480 (CCL-228), and Caco2 (HTB-37) were acquired from American Type Culture Collection (ATCC, Manassas, Virginia, USA), authenticated, according to ATCC instructions. MC38 (ENH204-FP) was acquired from Kerafast and NCM-460 (CVCL_0460) from INCELL. All cell lines were cultured in an incubator set at 37 °C in 5% CO2 and 95% atmospheric air, maintained with DMEM (Gibco; cat. no. 11965118) supplemented with 10% (v/v) Fetal Bovine Serum (Gibco; cat. no. 16140071) and Antibiotic-Antimycotic (Gibco; cat. no. 15240112). All cell lines were assessed regularly to ensure they were free of mycoplasma contamination.

CRISPR/Cas9 knockout

To knockout YTHDF1, we designed independent single guide RNAs (sgRNAs) using the CRISPR tool (http://crispr.mit.edu) and had them constructed into vector pSpCas9(BB)-2A-Puro (PX459) V2.0 (Addgene; #62988), following the instructions on Addgene. The following sgRNA sequences against murine *YTHDF1* were used: sgRNA1 (KO1): ATCCCGTATCTCACTACCTA; sgRNA2 (KO2): ATTTCCTTACTCCCTCAGCG. A nontargeting sequence GTAACCTCTCGAGCGATAGA was used in the control vector (NC). To generate the knockout clones, MC38 or CT26 cells were transfected with the constructed vector using Lipofectamine LTX (Thermo Fisher Scientific; cat. no. 15338030), according to the manufacturer's instructions. One day after the transfection, the cells were selected with puromycin at 5 or 8 μg/ml for MC38 or CT26, respectively. The selected cells were then trypsinized, and 2000 cells were plated in one well of a 6-well dish in one ml of growth medium. Single cells were collected using a pipette on a microscope and seeded to a well of a 96-well dish containing growth medium. Medium was refreshed every 5-7 days, and after a total of 10-16 days' culture single cells that grew into colonies were expended to dishes with a bigger format. Clones validated to show loss of YTHDF1 were used in the subsequent experiments.

Stable cell line with YTHDF1 overexpression

Human wide type YTHDF1 or YTHDF1 mutant (K395A, Y397A) was cloned into pLenti CMV Blast empty (Addgene; #17486). The vectors were transfected to HEK293T for virus generation as described above, and DLD1 cells were infected by the virus at the presence of 4 μg/ml of polybrene. The infected cells were then selected with blasticidin S (Thermo Fisher Scientific; cat. no. A1113903) at 5 μg/ml, and the cells were subjected to further analyses after the selection.

Syngeneic mice models

All experimental protocols were conducted after approval by Department of Health, The Government of the Hong Kong Special Administrative Region, and by University Animal Experimentation Ethics Committee, The Chinese University of Hong Kong. MC38 and CT26 cells resuspended in PBS were 1:1 (v/v) mixed with matrigel (BD Biosciences; cat. no. 354248) and subcutaneously injected to 6–8-week-old male C57BL/6 and BALB/c, respectively. The cells were injected at one million cells in a total volume of 50 μl per injection. Mice were acquired from The Chinese University of Hong Kong and a minimum of five mice were used per group. Assessment of tumor size began 6–8 days after cell inoculation and was performed once every 2–4 days using calipers. Tumor volume was calculated with the formula: $V = (d^2 \times D)/2$, where d stood for minor tumour axis and D for major tumour axis; and the data was presented as mean ± s.e.m. in mm^3. All mice were maintained at 21 °C ± 1, 55 to 70% humidity, and with a 12 h light/ dark cycle, from 7 am to 7 pm.

Reverse transcription-quantitative PCR (RT-qPCR)

RNAs were isolated with Trizol reagent (Thermo Fisher Scientific) and converted into cDNA using the PrimeScript RT Reagent Kit (Takara; cat. no. RR037B) and a 96-Well thermal cycler (Applied Biosystems). Quantitative PCR (qPCR) was performed with One-Step TB Green PrimeScript RT-PCR Kit II (Takara; cat. no. RR086B), according to the instructions from the manufacturer. The assays were conducted in technical triplicates in the ViiA7 Real-Time PCR System (Thermo Fisher Scientific) in a 96- or 386-well plate format. *ACTB* was used as an internal control. Relative expression levels were examined using the $2^{-\Delta\Delta C}$T method. Gene-specific primers used in this study are shown in **Table S3**.

Immunohistochemistry

After embedded in paraffin, tumor samples were sectioned, deparaffinized, and rehydrated. Antigens were then retrieved with sodium citrate buffer (10 mM sodium citrate, 0.05% tween 20, pH 6.0), and the sections were treated with 3% H_2O_2 and blocked with 5% goat serum. The sections were then incubated with anti-p65 (Cell Signaling Technology; cat. no. 8242) overnight at 4 ℃, followed by incubation with Goat Anti-Rabbit IgG (H + L)-HRP Conjugate (1706515, Bio-Rad). The sections were further counterstained with hematoxylin. Images were acquired using a microscope and three random images for each tumor were used for quantification. The quantification was conducted with the brown layer deconvoluted from the image, using (Fiji Is Just) ImageJ downloadable online (https://imagej.net/software/fiji/downloads).

Immunofluorescence

Tumor samples were frozen with liquid nitrogen in TissueTek OCT Compound (Sakura Finetek) and stored at -80 ℃. The frozen tissue blocks were sectioned into 5 μm thickness and the sections were fixed with pre-cooled acetone or 4% paraformaldehyde for 10 mins, for MDSC or T cell detection, respectively. The sections were further permeabilized with 0.25% Triton X-100 for 15 mins, blocked with 5% goat serum, and incubated with specific antibodies with 1% goat serum overnight at 4 ℃. The sections were then washed with PBS twice, stained with Hoechst 33342 (Thermo Fisher Scientific; cat. no. H3570), and further washed with PBS for three times, followed by mounting with ProLong™ Glass Antifade Mountant (Thermo Fisher Scientific; cat. no. P36980). The fluorescence images were acquired with the Leica TCS SP8 multiphoton system. The following antibodies from Biolegend were used: Alexa Fluor® 594 anti-mouse Gr-1 (clone RB6-8C5), Alexa Fluor® 594 anti-mouse CD8a (clone 53-6.7), Alexa Fluor® 594 anti-mouse CD4 (clone GK1.5), Alexa Fluor® 488 anti-mouse CD3 (clone 17A2), and Alexa Fluor® 488 anti-mouse/human CD11b (clone M1/70).

Western blot

Cells were lysed using 4% (w/v) sodium dodecyl sulfate solution, and the protein concentration was assessed using the Pierce™ BCA Protein Assay Kit (Thermo Fisher Scientific; cat. no. 23227) following the manufacturer's instructions. Same amount of protein from each sample was loaded and separated using SDS-PAGE and transferred to PVDF membrane (Merck; cat. no. IPVH00010). The membrane was then blocked

using 5% (w/v) BSA or milk, incubated with specific primary antibody, and blotted with horseradish peroxidase (HRP)-linked secondary antibody, according to the manufacturer's instructions. Visualization was performed using chemiluminescent substrate (Thermo Fisher Scientific; cat. no. 34096) on the ChemiDocTM XRS + Imaging System (Bio-Rad). Primary antibodies were diluted at 1:1000, while secondary antibodies at 1:3000. The following antibodies anti-IκBα (cat. no. 4814), anti-p-IκBα (cat. no. 2859), anti-IKKα (cat. no. 11930), anti-p-p65 (cat. no. 3033), anti-p65 (cat. no. 8242), anti-histone H3 (cat. no. 9715), anti-p50 (cat. no. 3035), anti-β-actin (cat. no. 4970), HRP-linked anti-mouse IgG (cat. no. 7076), HRP-linked anti-rabbit IgG (cat. no. 7074) were acquired from Cell Signaling Technology, while anti-YTHDF1 antibody (cat. no. ab220162) was acquired from Abcam.

Enzyme-linked immunoassay (ELISA)

ELISA against murine (ab216951) and human CXCL1 (ab190805) were both acquired from Abcam and used according to the user manuals. Supernatant samples collected from in vitro cell culture were used without dilution, while tumor lysates and sera were used after dilution of five times prior to assessment.

RNA interference

To generate stable cell lines expressing shRNAs, the shRNAs were cloned into pLKO.1-puro vector (Addgene; cat. no. 8453) following the protocol provided on the Addgene website (http://www.addgene.org/tools/protocols/plko/). A pair of shRNAs that did not target any know human genome were used as negative control and was designated as shNC. shRNAs that targeted YTHDF1 were designated shYTHDF1. To generate viruses containing the shRNAs, HEK293T was transfected, using Lipofectamine 2000 (Invitrogen; cat. no. 11668019), with the shRNA-pLKO.1-puro vector and the viral packaging vectors pMDLg/pRRE (Addgene; cat. no. 12251), pRSV-REV (Addgene; cat. no. 12253), and pMD2.G (Addgene; cat. no. 12259). Media containing the viruses were collected 48–72 h post-transfection and filtered with 0.22 μm filter to remove cell debris. Target cells were infected with the viruses in addition with 4 μg/ml of polybrene (Sigma-Aldrich; cat. no. H9268). One day after the transduction, the cells were selected with appropriate concentration of puromycin for further experiments. The targeted sequences of the shRNAs were listed in **Table S4**.

Antibodies treatments

The anti-mouse PD1 (clone RMP1-14), anti-mouse CD8α (clone 2.43), and their isotype controls were all acquired from BioXcell. Randomization was performed when therapeutic effects had to be assessed in the experiments with anti-PD1. Anti-PD1 was administrated intraperitoneally at 100 μg per mouse for MC38 xenografts and 250 μg for CT26 xenografts, at days 7, 10, 13, 16, and 19. To deplete $CD8^+$ T cells in the immunocompetent mice, anti-mouse CD8α was injected intraperitoneally 4, 7, and 9 days after cancer cell inoculation, with a loading dose of 400 μg per mouse and 100 μg per mouse subsequently. The efficacy of $CD8^+$ T cell depletion was determined by measuring the fraction of $CD8^+$ T cells in the bloodstream of mice with flow cytometry analysis, one day after the last dose of anti-mouse CD8α treatment.

Vesicle-like PLGA-based nanoparticle (VNP) formulation

Vesicle-like PLGA-based nanoparticle were assembled by Guangzhou Kelan Biotechnology Co., Ltd (Guangzhou, China). 2'-O-Methyl (2'-OMe) modified siRNA with 2'-O-Methyl (2'-OMe) modification were purchased from GenePharma Co. Ltd (Shanghai, China). The sequencing of human YTHDF1 siRNA: sense (CCACUCAAACUCUUUCGGGTT), antisense (CCCGAAAGAGUUUGAGUGGAA); Mouse YTHDF1 siRNA: sense (GCACUGACUGGUGUCCUUUTT), antisense (AAAGGACACCAGUCAGUGCTT). For syngeneic tumor models, MC38 murine CRC cells and HCT116 human CRC cells were respectively injected into C57BL/6 mice (1×10^6 cells/mouse) and $CD34^+$ humanized mice (5×10^6 cells/mouse), VNP-siNC/siYTHDF1 were treated via intertumoral injection (40ug/mouse every 2 days) when tumors reached at 50~100 mm^3. Tumor weight and tumor volume were monitored and measured, the composition of immune cells in tumors were analysed by flow cytometry.

Flow cytometry analysis

Xenografts were cut into small pieces with a surgical blade, and digested with collagenase D (Roche; cat. no. COLLD-RO) at 0.5 mg/ml and DNase I (Roche; cat. no. 10104159001) at 0.25 mg/ml, at 37 ℃ for one hour with agitation. For measuring $CD8^+$ T cells in the bloodstream of mice after anti-CD8α treatment, 100 μl of blood was

collected retro-orbitally into a tube containing 50 µl 0.5 M EDTA solution (pH 8.0) The suspensions were then filtered with 70 µm cell strainers, blocked with anti-mouse CD16/32 (Biolegend; cat. no. 156604), and stained with Zombie Green™ Fixable Viability Kit (Biolegend; cat. no. 423112) and specific antibodies in PBS containing 1% (w/v) BSA. Flow cytometry was conducted with FACS Celesta instrument and data was analysed with FlowJo V10. The following antibodies were acquired from Biolegend and used in the flow cytometry analysis: BV421 anti-mouse CD19 (clone 6D5), BV605 anti-mouse CD45 (clone 30-F11), PE anti-mouse CD3 (clone 17A2), PE/Cy7 anti-mouse CD4 (clone RM4-5), BV711 anti-mouse CD8α (clone 53-6.7), BV421 anti-mouse Ly-6C (clone HK1.4), PE anti-mouse Gr-1 (clone RB6-8C5), PE/Cy5 anti-mouse CD11b (clone M1/70), PE/Cy7 anti-mouse Ly-6G (clone 1A8), BV711 anti-mouse IFN-γ (clone XMG1.2), BV421 anti-mouse CD8α (clone 53-6.7), PE anti-mouse granzyme B (clone QA16A02), PE/Cy5 anti-mouse CD3 (clone 17A2). Compensation was performed using single-color controls which were acquired by incubating the AbC™ Total Antibody Compensation Bead Kit (Thermo Fisher Scientific; cat. no. A10513) with the fluorochrome-conjugated antibodies.

RNA-sequencing

Total RNAs were extracted and purified with RNeasy Mini Kit (Cat. #74106; QIAGEN). The libraries were sequenced using the illumina HiSeq 4000 (PE150) according to the protocol from company (Novogene, China). FPKM (Fragments per Kilobase of transcript per Million mapped reads) using DESeq2 were used for calculating gene expression levels. WebGestalt (http://www.webgestalt.org) was utilized for pathway analysis of RNA-seq data. Pathway analysis was performed with Over-Representation Analysis (ORA) on KEGG database or WikiPathways database.

T cell suppression assay

The leukocytes were collected from allograft tumors with or without YTHDF1 knockout digesting by collagenase IV (Gibco, 0.5 mg/ml) and DNase I (Worthington, 0.25 mg/ml). MDSCs were isolated from leukocyte using EasySep™ Mouse MDSC ($CD11b^+Gr1^+$) Isolation Kit (STEMCELL). Autologous spleen was used for T cells isolation by EasySep™ Mouse T Cell Isolation Kit (STEMCELL), and then isolated T cells were labeled with carboxyfluorescein succinimidyl ester (CFSE) (Invitrogen).

CFSE-labeled T cells were co-cultured with MDSC cells at 96-well plates (T:MDSC=1:0 and 1:1) for 72 h, Dynabeads ™ Mouse TActivator CD3/CD28 (ThermoFisher) and IL-2 (BioLegend) was added into medium for culture. CFSE intensity were quantified by flow cytometry.

MDSC isolation and migration assay

EasySep™ Mouse MDSC ($CD11b^+Gr1^+$) Isolation Kit (STEMCELL) were used for MDSCs isolation from the spleens of CT26 tumor-bearing BALB/c or MC38 tumor-bearing C57BL/6 mice. MDSCs (1 x 10^5 cells/well) were seeded in the top chamber of the transwell (pore size: 0.8 μm), and the bottom chamber were filled with conditioned medium (CM, without FBS) which cultured CT26 or MC38 cells with or without YTHDF1. MDSCs migrated to the bottom chamber after 4 h incubation, and cells number were counted.

Cytokine multiplex immunoassay

The cytokine multiplex immunoassay was performed with the Mouse Cytokine 23-plex Assay (Bio-Rad; cat. no. M60009RDPD) on the Bio-Plex 200 System (Bio-Rad) according to the user guide. Three types of materials derived from MC38 or CT26 clones bearing YTHDF1 knockout were subjected to the assay. These include supernatants collected from cells cultured in vitro, tumor lysates derived from the subcutaneous xenografts, and sera from the mice bearing the subcutaneous xenografts. Supernatants were performed without dilution while tumor lysates and sera were diluted five times prior to assessment. Data was shown as value normalized to control, the NC clone. For data from tumor lysates or sera, the mean derived from four mice each group was shown.

Ribosome-sequencing

Cells with or without YTHDF1 knockout were treated with 100 μg/ml cycloheximide (CHX) for 5 min at 37°C. The unprotected mRNA regions in the cells were excluded by treating with RNAse I. According to the ribosome-sequencing (Ribo-seq) protocol from company (Novogene, China), The intact mRNA-ribosome complexes were sequenced by using illumina HiSeq 4000 (SE50). Reads mapping on human rRNAs, snoRNAs, snRNAs and tRNAs from GENCODE project (v30) were excluded. The

residual reads were mapped on the human genome via bowtie2 (version 2.3.4.3) with option -L 10. The featureCounts (version 1.6.4) with the parameters (M –fracOverlap 0.4 –largestOverlap) was utilized for calculating the expression of protein-coding genes. Pathway analysis of Ribo-seq was applied via *Gene Set Enrichment Analysis* (*GSEA*) methods.

MeRIP-sequencing and MeRIP-qPCR

Total RNAs were extracted with Trizol reagent (Thermo Fisher Scientific) and DNA contamination was removed using the DNase and DNase Buffer in the PrimeScript RT Reagent Kit (Takara; cat. no. RR037B). The RNAs were then fragmented with RNA Fragmentation Buffer (10 mM Tris-HCl, 10 mM $ZnCl_2$) for 5 min at 70°C. The fragmented RNAs were then incubated with the Protein A/G Magnetic Beads (HY-K0202, MedChemExpress) bound with the anti-m6A antibody (ab208577, Abcam) at 4°C for 4 hrs, at the presence of RNase inhibitor (10777019, Thermo Fisher Scientific). The beads were then washed twice in IP buffer (150 mM NaCl, 10 mM Tris-HCl, pH 7.5, 0.1% IGEPAL CA-630), twice in low-salt IP buffer (50 mM NaCl, 10 mM Tris-HCl, pH 7.5, 0.1% IGEPAL CA-630), and twice in high-salt IP buffer (500 mM NaCl, 10 mM Tris-HCl, pH 7.5, 0.1% IGEPAL CA-630). The RNAs were then eluted from the beads with the RLT buffer supplied in the RNeasy Mini Kit (74106, QIAGEN) and purified with the DireCTzol RNA Miniprep Kit (R2050, Zymo Research). The isolated RNAs were then subjected to RT-qPCR using the RT-qPCR procedures described above or RNA-sequencing. IGEPAL CA-630 (I8896) and $ZnCl_2$ solution (39059) were acquired from Sigma. The list of qPCR primers used in MeRIP-qPCR was in **Table S5**.

RIP-sequencing or RIP-qPCR

RIP was performed using anti-YTHDF1 antibody (Abcam, ab220162) and the EZ-Magna RIP™ RNA-Binding Protein Immunoprecipitation Kit (17-701, Sigma) according to the manufacturer's instructions. Briefly, cell pellets were lysed with the RIP Lysis Buffer. The cell lysates were then incubated with magnetic beads bound with the anti-YTHDF1 antibody overnight at 4°C. The beads were then washed with the RIP Wash Buffer for a total of 6 times and the RNAs were released by digesting the antibody with proteinase K in 1% (w/v) SDS at 55°C for 30 min. The RNAs then were isolated with phenol:chloroform:isoamyl alcohol (BP1754I-100, Fisher) and RNA precipitation

by ethanol. The resuspended RNAs were then subjected to RT-qPCR using the RT-qPCR procedures described above or RNA-sequencing.

Measurement of liver or kidney function indicators

Creatinine, blood urea nitrogen, alanine aminotransferase, and aspartate transaminase were measured in serum from the VNP-treated animals, using the Catalyst One Chemistry Analyzer (IDEXX) following the instructions from the user manual. Thirty microliters of each serum sample were diluted with PBS to a total volume of 120 μl, and then loaded to specific catalyst slides. The slides were then read with the analyzer automatically.

Statistical analysis

All measurements were acquired using distinct samples rather than collected with repeated measurements. GraphPad Prism version 8 (GraphPad Software; San Diego, CA) was used for data analysis, and the data were shown as means ± s.d., unless stated otherwise. Two-tailed student's t-test was used to conduct statistical analysis, unless stated otherwise. A *P* value lower than 0.05 was regarded as statistically significant, unless stated otherwise.

Figure S1

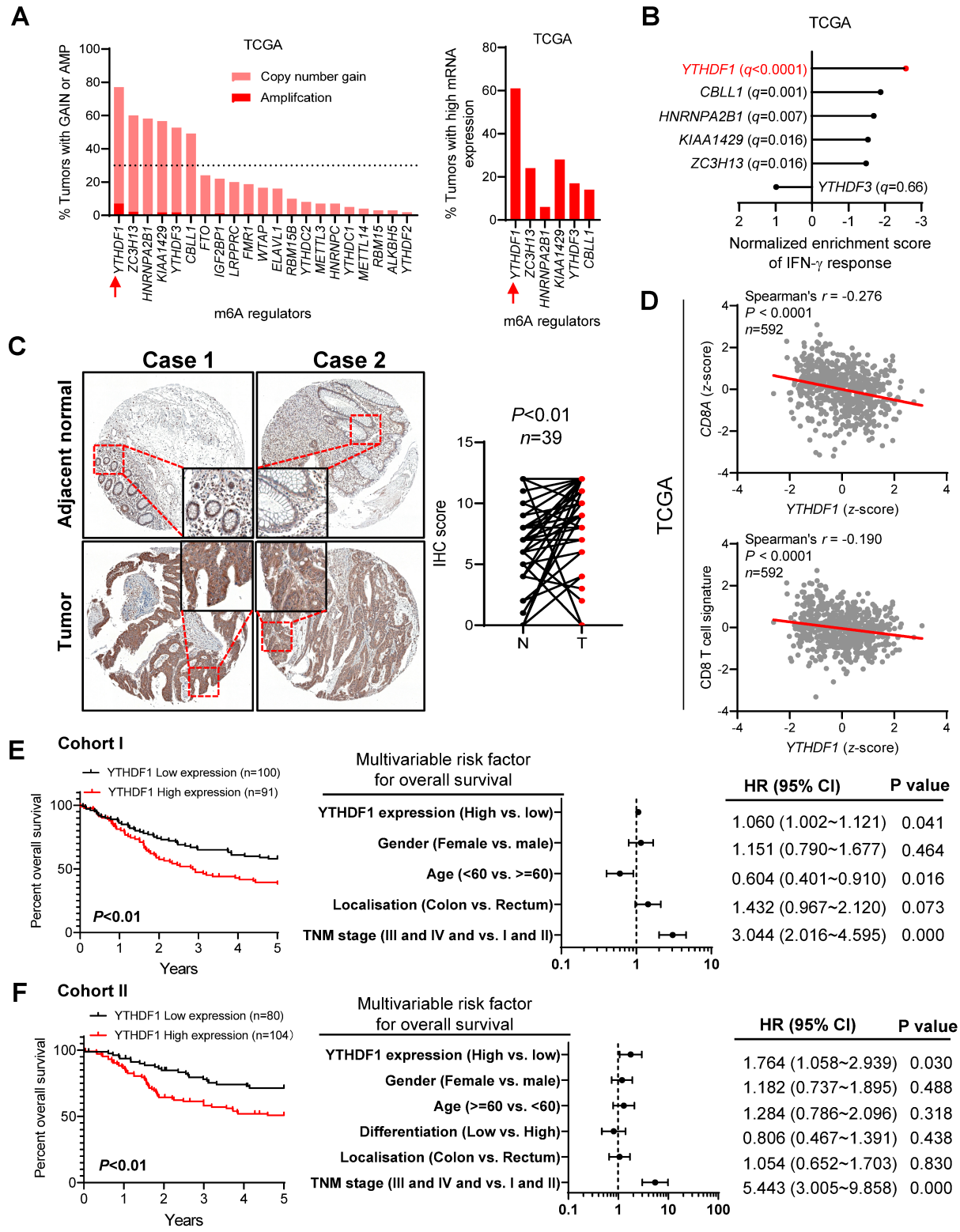

Figure S1. (**A**) Left: Percentage of tumors (*n*=526) that display copy number gain (GAIN) or amplification (AMP) of the indicated m6A regulators. Right: Percentage of tumors that display high mRNA expression of the indicated m6A regulators. High mRNA expression was defined as equal to or greater than two s.d. above the mean of diploid samples. (**B**) Gene set enrichment analysis (GSEA; *n*=524) for signature of IFN-γ response with the indicated m6A regulators. FDR lower than 0.0001 was highlighted in red. (**C**) Representative images and quantification of IHC comparing YTHDF1 expression between adjacent normal tissue and tumor tissue in cohort II. (**D**) Correlation of *YTHDF1* expression and *CD8A* expression or CD8 T cell signature in colorectal cancer. Data in **A**, **B**, and **D** were from TCGA. (**E**) In cohort I, patients with high expression of YTHDF1 (*n*=91) have a poor prognosis than those with low expression (*n*=100) based on the log-rank test. Multivariate Cox regression analyses illustrated that YTHDF1 was an independent prognostic factor in CRC (*P*<0.01). (**F**) In cohort II, patients with YTHDF1 high expression (*n*=104) had a poor prognosis than patients with low expression (*n*=80) according to the log-rank test (*P*<0.01). Multivariate Cox regression analyses revealed that YTHDF1 was an independent prognostic factor in CRC.

Figure S2

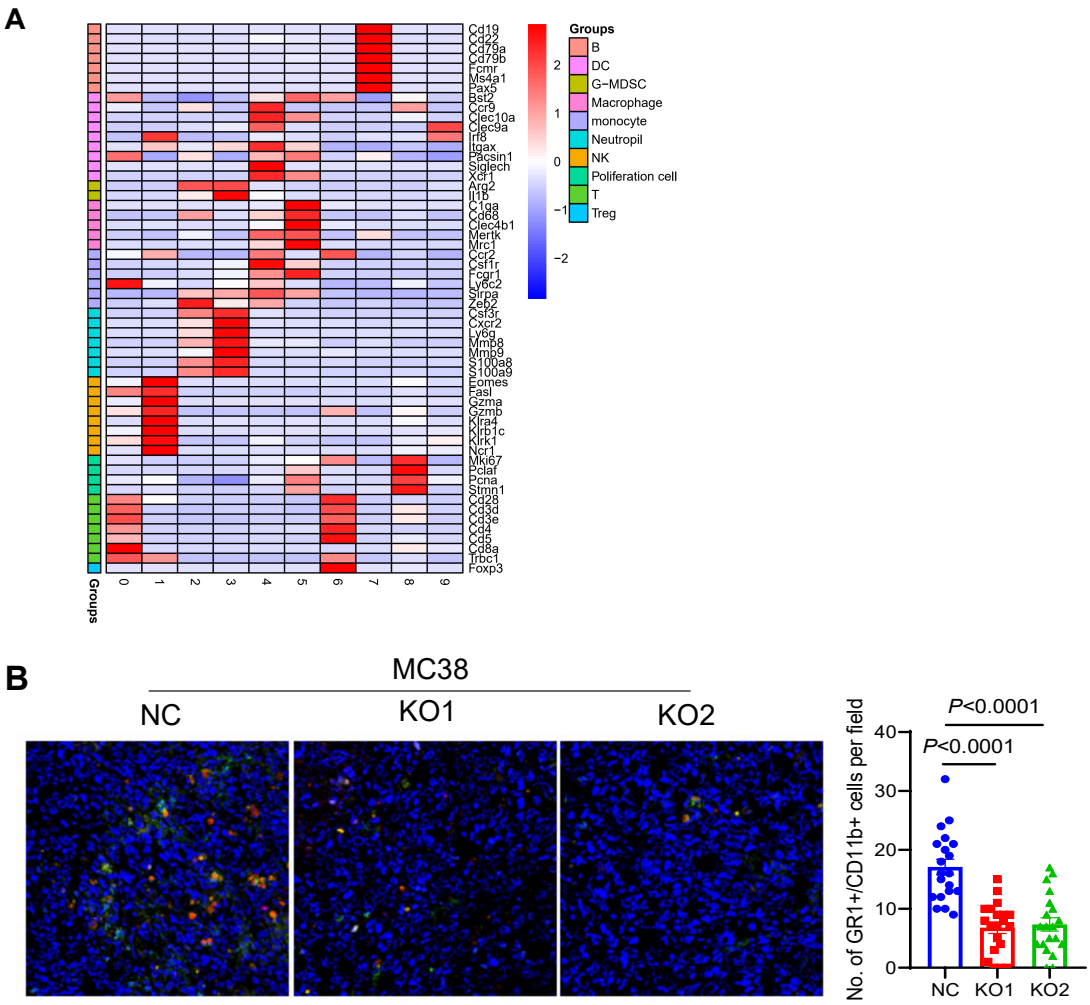

Figure S2. (**A**) Heatmap displaying the scaled expression patterns of top marker genes within CD45^{+} cells from wildtype mice. Red: high expression; Blue: low expression. (**B**) Immunofluorescence identifying MDSCs in subcutaneous tumors from C57BL/6 injected with the indicated MC38 cells. Red: CD11b. Green: Gr1. Blue: DAPI. [Two tailed t-test (B)].

Figure S3

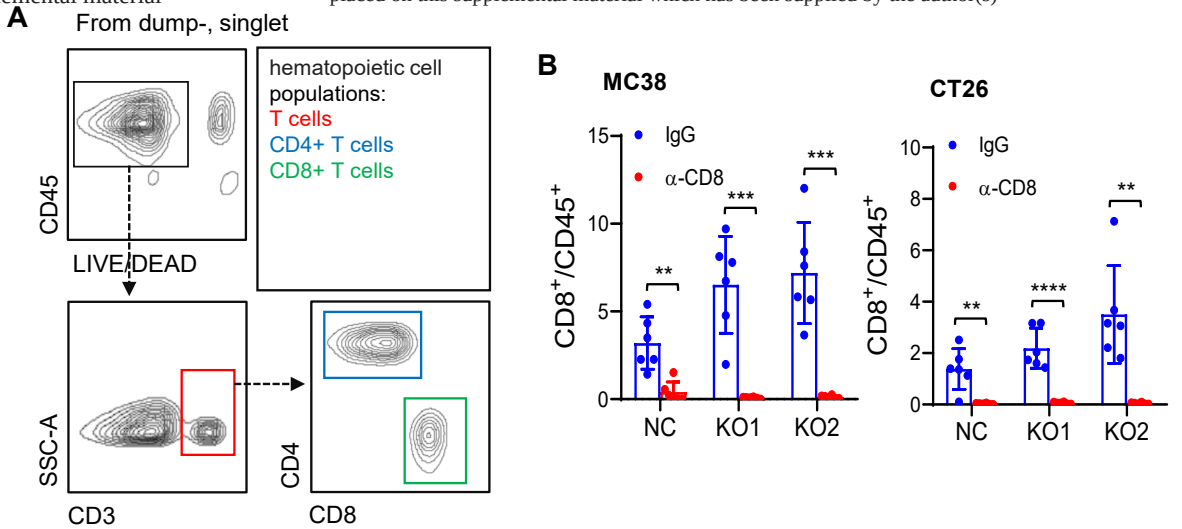

Figure S3. (**A**) Gating strategies to identify $CD4^+$ or $CD8^+$ T cells in the blood collected from mice. (**B**) Flow cytometry analysis on $CD8^+$ T cells in blood from mice injected subcutaneously with MC38 or CT26. $CD8^+$ T cells depletion was performed with anti-mouse CD8 antibody (α-CD8) at 200 μg/mouse once every three days. [Two tailed t-test (B)].

Figure S4

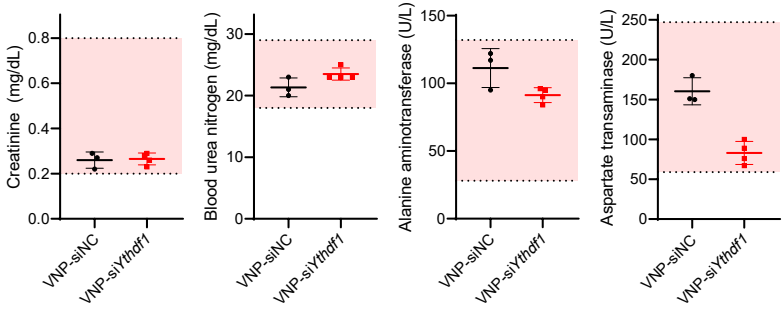

Figure S4. Serum markers from CD34$^+$ humanized mice bearing HCT116 tumors that were treated with the indicated vesicle-like nanoparticles (VNP). Pink box indicates the reference interval of each indicator.

Figure S5

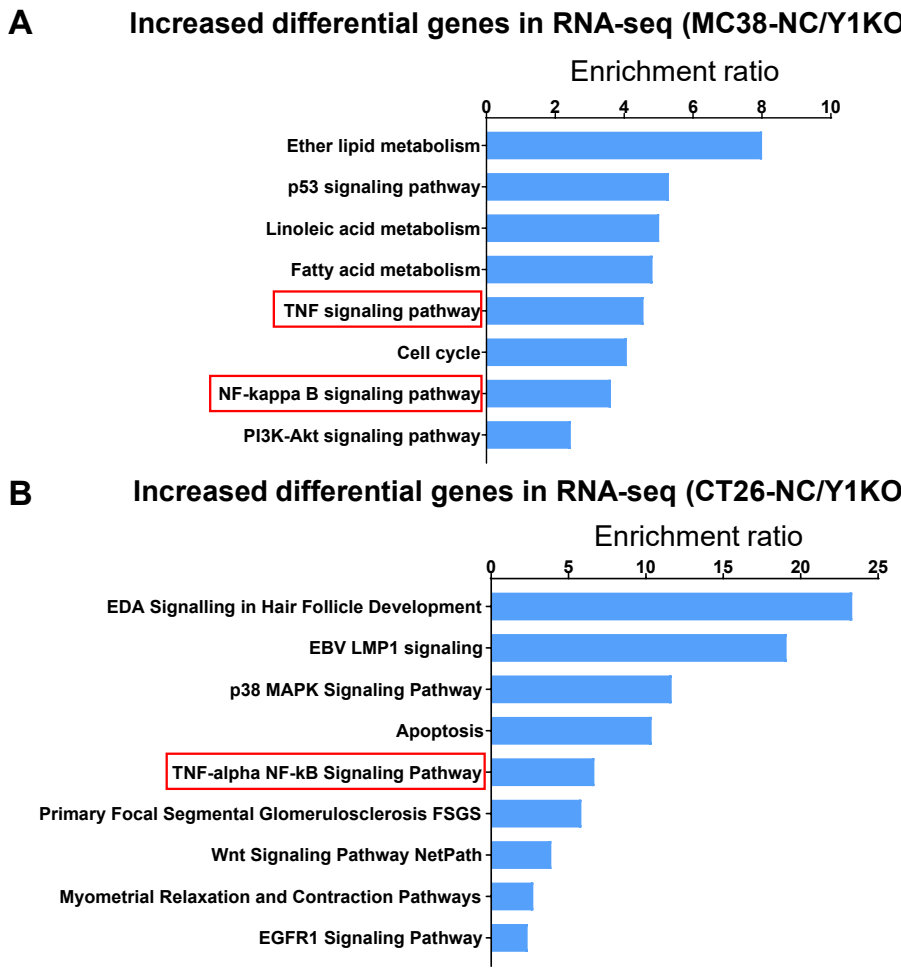

Figure S5. Increased differential genes (NC/Y1KO) were enriched in TNF/NF-κB signaling pathway. (**A**) Pathway analysis (KEGG) for increased differential genes of RNA-seq in MC38-NC compared to MC38-Y1KO. (**B**) Pathway analysis (Wikipathway) for increased differential genes of RNA-seq in CT26-NC compared to MC38-Y1KO. Y1KO: *Ythdf1* knockout.

Figure S6.

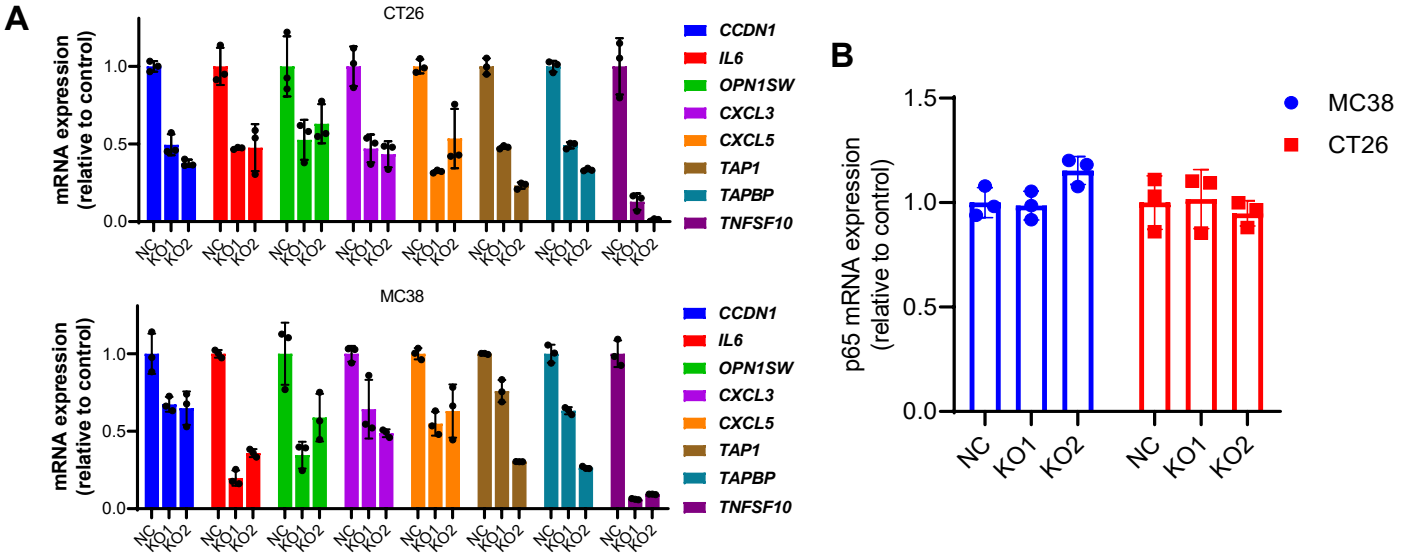

Figure S6. (**A**) RT-qPCR measuring mRNA expression of genes reported to be NF-κB targets in the indicated MC38 or CT26 clones. (**B**) RT-qPCR measuring p65 mRNA level in the indicated MC38 or CT26 clones. Data was acquired from technical triplicates. NC: control; KO: *Ythdf1* KO.

Figure S7.

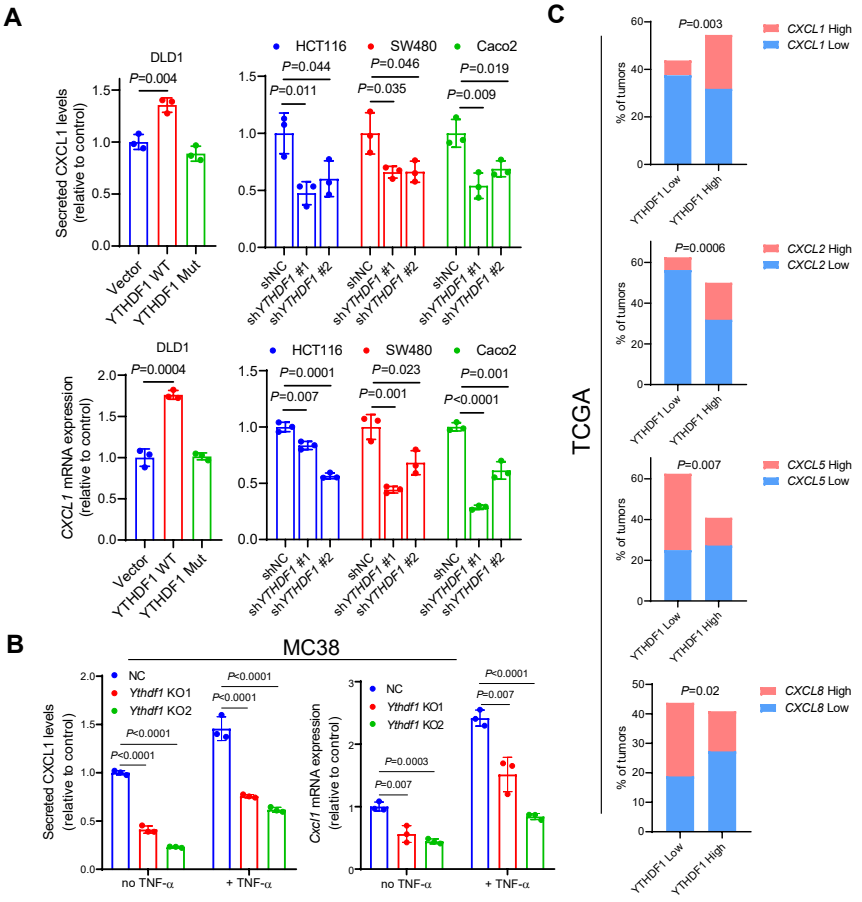

Figure S7. (**A**) RT-qPCR measuring *CXCL1* mRNA levels (top) and ELISA measuring CXCL1 secretion in supernatant (bottom) with the indicated human CRC cells. (**B**) Secreted CXCL1 levels measured by ELISA (left) and *Cxcl1* mRNA expression measured by RT-qPCR (right) in control or *Ythdf1*-depleted MC38 treated with or without TNF-α at 10ng/ml for eight hours. (**C**) Association between the expression of *YTHDF1* and CXCL1 or other CXCL family members in stage IV tumors (*n*=85) from TCGA CRC dataset. YTHDF1 Low: *n*=16; YTHDF1 High: *n*=22. [Two-tailed t tests in (B and C); chi-square tests in (D)]

Figure S8

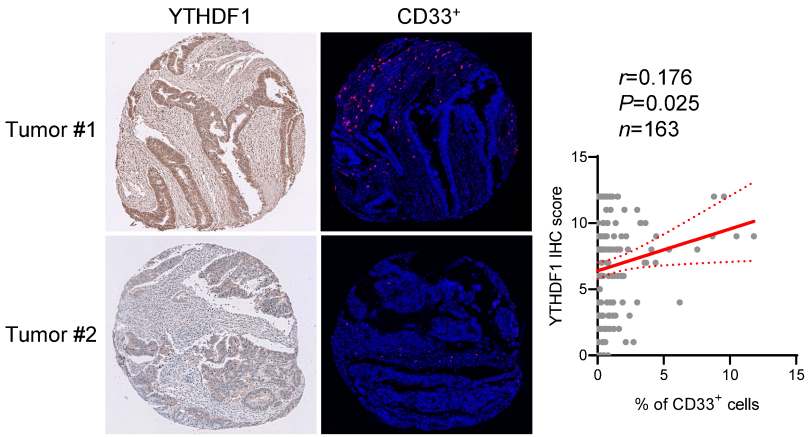

Figure S8. Representative images (left) of IHC of YTHDF1 and immunofluorescence of CD33 on CRC tissue microarray (n=163) from cohort I. Right panel: correlation of YTHDF1 IHC score and percentage of $CD33^+$ cells. All statistics were determined with Pearson correlation test.

Figure S9

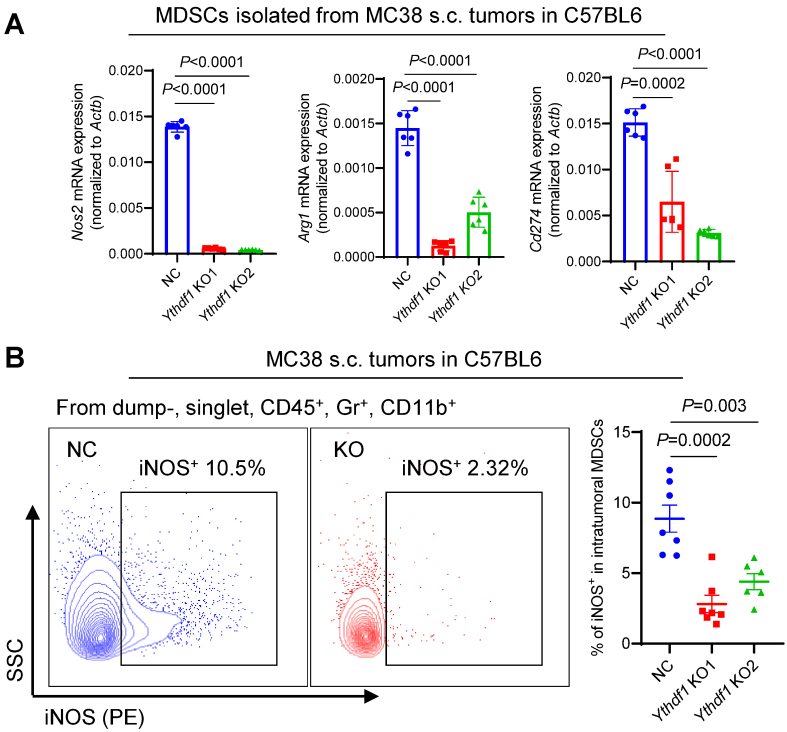

Figure S9. (**A**) mRNA expression of MDSC functional markers (*iNos*, *Arg1*, *Cd274*) in MDSCs isolated from *Ythdf1*-WT and *Ythdf1*-KO MC38 allografts. (**B**) Representative images (left) and quantification (right) of iNOS$^+$ MDSCs in *Ythdf1*-WT or *Ythdf1*-KO MC38 allografts by flow cytometry. [Two tailed t-test (A and B)].

Table S1. Clinical feature of CRC patients (Cohort I)

Clinical feature	High expression (n=91)	%	Low expression (n=100)	%
Age	67.9±10.7		66.6±13.9	
Gender				
M	43	47.3	64	64.0
F	48	52.7	36	36.0
TNM				
I	5	5.5	12	12.0
II	24	26.4	35	35.0
III	26	28.6	30	30.0
IV	36	39.5	23	23.0
Localization				
Colon	57	46	61	35.2
Rectum	34	54	39	64.8

Table S2. Clinical feature of CRC patients (Cohort II)

Clinical feature	High expression (n=104)	%	Low expression (n=80)	%
Age	57.9±11.8		59.7±12.4	
Gender				
M	61	58.7	42	52.5
F	43	41.3	38	47.5
TNM				
I	5	4.8	11	13.7
II	38	36.5	34	42.5
III	57	54.8	30	37.5
IV	4	3.9	5	6.3
Localization				
Colon	57	54.8	42	52.5
Rectum	47	45.2	38	47.5
Differentiation				
Low	31	29.8	22	27.5
High	73	70.2	58	72.5

Table S3. Primer sequences for qPCR

Species	Target gene	Forward/ Reverse	Sequence (5' to 3')
Mus musculus	*ACTB*	Forward	GGCCAACCGTGAAAAGATGA
Mus musculus	*ACTB*	Reverse	TACGACCAGAGGCATACAGG
Mus musculus	*RELA* (p65)	Forward	CCGGGATGGCTACTATGAGG
Mus musculus	*RELA* (p65)	Reverse	TCTTCACACACTGGATCCCC
Mus musculus	*CXCL1*	Forward	TCCAGAGCTTGAAGGTGTTGCC
Mus musculus	*CXCL1*	Reverse	AACCAAGGGAGCTTCAGGGTCA
Mus musculus	*CXCL3*	Forward	TACGATCAGCGCCTCAATGCCA
Mus musculus	*CXCL3*	Reverse	AGCAGGAAACCAGCCACTAGCT
Mus musculus	*CXCL5*	Forward	CCGCTGGCATTTCTGTTGCTGT
Mus musculus	*CXCL5*	Reverse	CAGGGATCACCTCCAAATTAGCG
Mus musculus	*CCND1*	Forward	GGAGATTGTGCCATCCATGC
Mus musculus	*CCND1*	Reverse	GACCTCCTCTTCGCACTTCT
Mus musculus	*OPN1SW*	Forward	CTTACGGCTTGTCACCATCC
Mus musculus	*OPN1SW*	Reverse	CCTGCACACCATCTCCAGAA
Mus musculus	*TAPBP*	Forward	CAGCACTCTCTTCAGCCTCT
Mus musculus	*TAPBP*	Reverse	GTTATGGGTGAGGACGGTCA
Mus musculus	*TAP1*	Forward	CCTGGGCCCTAAGAAGAGAC
Mus musculus	*TAP1*	Reverse	GAATCCAGTCAGTGATGCGG
Mus musculus	*TNFSF10*	Forward	TGTGTCTGTGGCTGTGACTT
Mus musculus	*TNFSF10*	Reverse	TCCCAGAAATCCTCATCCGT
Mus musculus	*IL6*	Forward	AGCCAGAGTCCTTCAGAGAGAT
Mus musculus	*IL6*	Reverse	GCCACTCCTTCTGTGACTCC
Homo sapiens	*CXCL1*	Forward	CACTCAAGAATGGGCGGAAA
Homo sapiens	*CXCL1*	Reverse	CCTTCTGGTCAGTTGGATTTGT
Homo sapiens	*ACTB*	Forward	CAACCGCGAGAAGATGACC
Homo sapiens	*ACTB*	Reverse	CCAGAGGCGTACAGGGATAG
Homo sapiens	*RELA* (p65)	Forward	CCGGGATGGCTTCTATGAGG
Homo sapiens	*RELA* (p65)	Reverse	CTGACTGATAGCCTGCTCCA

Table S4. Target sequence for shRNA

shRNA name	Target sequence (5' to 3')
shNC	TTCTCCGAACGTGTCACGT
sh*YTHDF1*-1	GATACAGTTCATGACAATGA
sh*YTHDF1*-2	CAGGCTGGAGAATAACGACAA

Table S5. Primer sequences for MeRIP-qPCR

Primer name	**Sequence (5' to 3')**
RELA-MeRIP#1 F	GACCCAGGAGTGTTCACAGA
RELA-MeRIP#1 R	AGCTGTGGAGTGAGACATGG
RELA-MeRIP#2 F	GGCTTCCCAATGGTCTCTCA
RELA-MeRIP#2 R	CACCTTAGGAGCTGATCTGACT
RELA-MeRIP#3 F	GCTTCCATCTCCAGCTTCTAG
RELA-MeRIP#3 R	GTGTACAGGAATCCGCGTG
RELA-MeRIP#4 F	ACAGGTGGGATGTTGCTGG
RELA-MeRIP#4 R	CCTGCCCTCCTGACTCTACA